

**FLUIDS AND LITHOLOGY PREDICTION THROUGH AVO
INVERSION, A CASE STUDY IN THE AA FIELD, WEST
NATUNA BASIN, INDONESIA**

THESIS

**AISYAH ANITA
NPM:0706171743**



**UNIVERSITY OF INDONESIA
FACULTY OF MATHEMATIC AND NATURAL SCIENCE
PHYSICS GRADUATE PROGRAM
JAKARTA
JULY, 2009**

PAGE OF APPROVAL

Name : Aisyah Anita
NPM : 0706171743
Thesis : Fluids and Lithology Prediction through AVO Inversion, a Case Study in the AA Field, West Natuna Basin, Indonesia

APPROVED AS TO STYLE AND CONTENT BY:

Chairman : Dr. Dedi Suyanto (.....)
Supervisor : Prof.Dr. Suprayitno Munadi (.....)
Examiner I : Dr. Abdul Haris (.....)
Examiner II : Dr. Adriansyah (.....)
Examiner III : Dr. Carlos Tarazona (.....)

**PHYSICS GRADUATE PROGRAM
FACULTY OF MATHEMATIC AND NATURAL SCIENCE
JAKARTA
JULI, 2009**

ABSTRACT

At AA Field, we applied seismic AVO inversion methods to generate acoustic impedance volume. The results of this approach provide not only better resolution for more accurate structural interpretations, but also allow us to perform better fluids and reservoir properties predictions.

Seismic AVO inversion transforms seismic data into P-impedance (product of density and P-wave velocity), S-impedance (product of density and S-wave velocity), and density (ρ) for better discrimination on fluid and lithology effects.

Prior to AVO Inversion, rock physics of the reservoir were analyzed for Fluid Replacement Modeling (FRM) purposes. Through this FRM, we employed Biot Gassmann fluid substitution to investigate fluid effects on rocks elastic properties. Initially, we setup input logs of V_p , V_s , ρ , and fluid saturation (S_w) with known fluid type. Later on the workflow, analysis was carried-out through comparison between well synthetic seismogram of different fluids or rock properties with seismic data using extracted wavelet. Different fluid with different rock properties exhibit different amplitude responses and characters.

This study has enhanced our seismic interpretation for fluid and lithology discriminations. Furthermore, this study can be used for optimization of oil and gas productions at AA Field.

ABSTRAK

Di lapangan AA, metoda seismik inversi digunakan untuk menghasilkan volume akustik impedansi. Hasil dari metode ini tidak hanya menghasilkan resolusi yang lebih baik untuk interpretasi struktur yang lebih akurat, tetapi juga memberikan pengertian lebih baik tentang prediksi sifat-sifat fluida dan reservoir.

Seismik inversi AVO merubah seismik data menjadi P-impedansi (hasil dari densitas dan kecepatan gelombang-P), S-impedansi (hasil dari densitas dan kecepatan gelombang-S), dan densitas (ρ) yang menjadikan pemisahan fluida dan litologi menjadi lebih baik.

Sebelum membahas AVO inversi, reservoir fisika batuan dianalisa untuk tujuan *Fluid Replacement Modeling* (FRM). Melalui FRM, dilakukan pertukaran fluida menggunakan persamaan Biot Gassmann untuk mengetahui pengaruh fluida pada sifat-sifat elastik batuan. Awalnya, V_p , V_s , ρ dan S_w dari suatu fluida harus diketahui. Kemudian, hasil analisa dibawa melalui perbandingan antara sumur seismogram sintesa dari fluida yang berbeda atau sifat-sifat batuan dengan data seismik menggunakan hasil ekstraksi wavelet. Perbedaan fluida dengan perbedaan sifat-sifat batuan menunjukkan perbedaan respons amplitudo dan karakternya.

Hasil studi ini diharapkan memperkuat interpretasi seismik untuk pemisahan fluida dan litologi. Selanjutnya, melalui studi diharapkan dapat digunakan untuk mengoptimalkan produksi oil dan gas dan di lapangan AA.

ACKNOWLEDGEMENTS

I would like to acknowledge and express my appreciation to the Management of 'X' Company for giving me permission to use the seismic and well data which made this study possible. I would like to thank to all friends in 'X' company for their valuable discussion and comments.

Special thank is given to Prof. Dr. Suprajitno Munadi, who is supervisor of my thesis for his advice and valuable discussion during finalizing my study and completing the thesis. Thank is given to my lecturers in University of Indonesia for support and valuable discussion. Thank is also given to Pak Parman who has made a smooth running of the study. I would like to thank my friends that are not possible to name one by one on this occasion.

Finally, I would like to express my sincere gratitude to my husband, my children, my parents and my sisters, who have provided me with endless love and support throughout my life.

Jakarta, July 2009

Aisyah Anita

Table of Contents

	Page
TITLE	
PAGE OF APPROVAL	i
ABSTRACT	ii
ACKNOWLEDMENT	iv
TABLE OF CONTENTS	v
TABLE OF FIGURES	vii
TABLE	x
CHAPTER I. INTRODUCTION	
1.1. Background	1
1.2. Goals	2
1.3. Area of The Study	2
1.3.1. Structural and Stratigraphy	2
1.3.2. Petroleum System of AA Field	3
1.3.2.1. Source Rock	3
1.3.2.2. Migration	4
1.3.2.3. Reservoir Rock	4
1.3.2.4. Trap	4
1.3.2.5. Seal	4
CHAPTER II. DATA AND METHODOLOGY	
2.1. Data	7
2.1.1. Log Data	7
2.1.2. Seismic Data	7
2.2. Methodology	8
2.2.1. Well Data	8
2.2.2. Well Log to Seismic Tie	9
2.2.3. AVO Inversion	9
2.3. Scope of Study	9

CHAPTER III. THEORY

3.1. Rock Physics	11
3.1.1. Density.....	12
3.1.2. Velocity	14
3.1.3. The Biot Gassmann Model	19
3.1.4. Relationship Between P and S Velocities	23
3.2. Acoustic in Reservoir Characterization	25
3.2.1. Class 1: High Impedance Gas Sand	26
3.2.2. Class 2: Near Zero Impedance Contrast Sand	26
3.2.3. Class 3: Low Impedance Gas Sand	27
3.2.4. Class 4: Anomaly	27
3.1.5. Acoustic Impedance And Reflectivity	29

CHAPTER IV. RESULT AND DISCUSSION

4.1. Petrophysical Analysis.....	31
4.2. Well Log to Seismic Correlation and Wavelet Extraction	34
4.2.1. Checkshot Corrections.....	35
4.2.2. Wavelet Extraction	36
4.3. AVO Modelling.....	40
4.3.1. Fluid Replacement Modelling Procedure	41
4.3.2. 2D Synthetics	46
4.4. AVO Inversion	48
4.4.1. Initial Guess Model	49
4.4.2. Prestack Inversion.....	51

CHAPTER V. CONCLUSION AND RECOMMENDATION

5.1. Conclusion	56
5.2. Recommendation	56

Table of Figures

	page
Figure-1.1: Location of AA field, West Natuna, Indonesia.	4
Figure-1.2: Stratigraphic Colomn in the AA field	6
Figure-2.1: Basemap of AA field	8
Figure-2.2: Flowchart of Fluids and Lithology Prediction Through AVO Inversion, a Case Study in the AA Field, West Natuna Basin, Indonesia	10
Figure-3.1: Rock properties are determined by matrix type, porosity, and fluid type	12
Figure-3.2: Wylli's equation applied to an oil and gas reservoir	13
Figure-3.3: A rock may be deformed by (a) compression, (b) tension, and (c) shear	14
Figure-3.4: Volumetric stress or cubicle dilatation.....	15
Figure-3.5: Poisson's ratio as a function of P-wave to S-wave ratio.....	17
Figure-3.6: P-wave velocity vs Water Saturation for both a gas sand and an oil sand.....	18
Figure-3.7: A plot of P-wave and S-wave velocity versus water saturation in a gas sand using the Biot Gassmann equation.....	20
Figure-3.8: A plot of Poisson's ratio versus water saturation in a gas sand....	21
Figure-3.9: A plot of P-wave and S-wave velocity of a function of water saturation on an oil filled sand.....	21
Figure-3.10: A plot of Poisson's ratio as a function of water saturation on an oil filled sand	22
Figure-3.11: P-wave velocity versus Poisson's ratio plot for a number of different water saturations.....	22
Figure-3.12: The mudrock line.....	23
Figure-3.13: Poisson's Ratio versus P-wave Velocity.....	24
Figure-3.14: V_p / V_s Ratio versus P-wave Velocity.....	24
Figure-3.15: Plot of Reflection Coefficient to Incident Angel in top of gas sand	25

Figure-3.16: Amplitude to offset – Rutherford and Wiliam classification by Rutherford and Williams	27
Figure-3.17: Reflektion coefficient of gas sandstone againts the offset for 4 classes of AVO anomaly	28
Figure-3.18: Crossplot of AVO intercept against gradient shows 4 possibilities of quadrant.....	29
Figure-4.1: P-Impedance versus Poisson's Ratio versus Porosity of AA-2...	32
Figure-4.2: P-Impedance versus Poisson's Ratio versus Porosity of AA-3....	33
Figure-4.3: P-Impedance versus Poisson's Ratio versus Porosity of AA-4.....	33
Figure-4.4: P-Impedance versus Poisson's Ratio versus Water Saturation of AA-4.....	34
Figure-4.5: P-Impedance versus Poisson's Ratio versus Porosity of AA-2, AA-3 and AA-4.....	34
Figure-4.6: Wavelet of AA-2 well in Time and Frequency Domains.....	37
Figure-4.7: Wavelet of AA-3 well in Time and Frequency Domains.....	37
Figure-4.8: Wavelet of AA-4 well in Time and Frequency Domains.....	38
Figure-4.9: The well to seismic correlation at the AA-2 well.....	38
Figure-4.10: The well to seismic correlation at the AA-3 well.....	39
Figure-4.11: The well to seismic correlation at the AA-4 well.....	39
Figure-4.12: Vp and Vs in a gas sand at AA-2 well using Biot Gasmann....	41
Figure-4.13: Vp and Vs in an oil sand at AA-3 well using Biot Gasmann....	42
Figure-4.14: Vp and Vs in an oil-water sand at AA-4 well using Biot Gasmann.....	42
Figure-4.15: Fluid Replacement Modeling of AA-2 with water saturation 50% and 100%.....	43
Figure-4.16: S-wave versus P-wave versus Density of AA-2 well (Insitu and and 100% Sw).....	44
Figure-4.17: Fluid Replacement Modeling of AA-3 with water saturation 50% and 100%.....	44
Figure-4.18: S-wave versus P-wave versus Density of AA-3well (Insitu and 100% Sw).....	45

Figure-4.19: Fluid Replacement Modeling of AA-4 with water saturation 50% and 100%.....	45
Figure-4.20: Fluid Replacement Modeling of AA-4 with water saturation 50% and 100%.....	46
Figure-4.21: 2D Synthetics of AA-2 well (Insitu and Wet Cases).....	47
Figure-4.22: 2D Synthetics of AA-3 well (Insitu and Wet Cases).....	47
Figure-4.23: 2D Synthetics of AA-4 well (Insitu and Wet Cases).....	47
Figure-4.24: Initial P-impedance and S-impedance Models showing AA-2 well location	50
Figure-4.25: Initial P-impedance and S-impedance Models showing AA-3 well location.....	50
Figure-4.26: Initial P-Impedance and S-impedance Models showing AA-4 well location.....	51
Figure-4.27: The fit between the inversion traces and the original logs for AA-2.....	52
Figure-4.28: The fit between the inversion traces and the original logs for AA-3.....	52
Figure-4.29: The fit between the inversion traces and the original logs for AA-4.....	53
Figure-4.30: Amplitude Zp versus Amplitude PR ..	54
Figure-4.31: Fluids and lithology distribution at AA-2 well.	54
Figure-4.32: Fluids and lithology distribution at AA-3 well ..	55
Figure-4.33: Fluids and lithology distribution at AA-34well	55
Figure-4.34: Horizon slice on Top Upper Cakalang of Zp volume	56
Figure-4.35: Horizon slice on Top Upper Cakalang of PR volume	56

TABLE

Table-4.1: Zone Boundary for AVO modelling 40



CHAPTER I

INTRODUCTION

1.1. Background

Seismic inversion is a technique that has been in used by geophysicists for almost forty years. Early inversion techniques transformed the seismic data into P-impedance (the product of density and P-wave velocity), from which we were able to make predictions about lithology and porosity. However, these predictions were somewhat ambiguous since P-impedance is sensitive to lithology, fluid and porosity effects, and it is difficult to separate the influence of each effect. To perform a less ambiguous interpretation of our inversion results, we must perform elastic inversion, in which we estimate P-impedance, S-impedance (the product of density and S-wave velocity) and density. The reason for this is that the P and S-wave response of the subsurface is sufficiently different to allow us to see the difference between fluid and lithology effects.

Around 1900, Knott and Zoeppritz developed the theoretical work necessary for AVO theory (Knott, 1899; Zoeppritz, 1919). Given the P-wave and S-wave velocities along with the densities of the two bounding media, they developed equations for plane wave reflection amplitude as a function of incident angle. However, the exact mathematical expression of the reflection coefficient is exceptionally long, thus making it difficult to perceive how reflection amplitude varies if a rock properties is changed slightly. Koefoed (1955) described the relationship of AVO to change in Poisson's ratio across a boundary. Koefoed's results were based on the exact Zoeppritz's equation. The conclusions drawn by Koefoed are the basic of today's AVO interpretation. Shuey (1985) developed the linear approximation equation, he was inspired to examine AVO after learning of Koefoed article. Shuey showed which

combination of rock properties were effective at successive ranges of incident angles. One of Shuey's main contribution is that he identified how various rock properties can be associated with near, mid, and far angle ranges.

However to describe AVO response, a complete description of the rock properties with detailed study of seismic amplitude is needed. The use of seismic data with optimum quality is important too and therefore we use partial angle stack (near mid and far) in this thesis because it can suppressed the noise and can correct the residual time alignment problems, especially at the zone of interest.

1.2. Objectives

Objectives of this thesis is to estimate acoustic impedance (AI) and Poisson ratio (PR) inversion of elastic parameter using partial angle stack to identify the distribution of lithology and fluids content. The second goal, through this study, the model is expected could be applied and tested to other exploration and/ or development field in other areas.

1.3. Area of the Study

1.3.1. Structural and Stratigraphy

The AA field is located at West Natuna Basin, South Natuna Sea. The basin formed during the Oligocene within an extensional faulting phase. This phase is related to the rifting in the South Natuna Sea area. The location of AA field can be seen in FIGURE-1.1. Predominantly granitic basement provided the provenance for coarse continental clastics, which filled in the basin. Paus and Cakalang sediments were deposited in fluvial and lacustrine environments during this period.

From late Oligocene to Middle Miocene, a compressive and wrenching phase caused structural inversion of the basin. It resulted in northwest-southeast trending right lateral movements in the Malay_Natuna Basins. Many original half-grabens were inverted into faulted anticlines (now major exploration target). Deposition continued in a marginal marine/estuarine setting with fluvial and marginal marine deposits of the Koi, Karper, and Upper Toman formations. Inversion ceased by the end of Middle Miocene and regional unconformity developed. Subsequently a regional sand phase dominated the structural regime. The resulting Gelodok shales are generally considered to be open shelf, shallow marine deposits. Tertiary stratigraphic chart for West Block “B PSC”, South Natuna Sea can be seen in FIGURE-1.2.

1.3.2. Petroleum System of AA Field

1.3.2.1. Source Rock

A good quality source rock is deposited in syn-rift sediment, primarily in Paus formation. Berendson (1991) revealed, instead of having a source rock, Paus formation provided a good quality of reservoir rocks. Generally, source rock is deposited in fluvial sediment with TOC between 0.06-6.4% (Fainstein, 1997). Generally, maturity of source rock in this formation will produce an oil hydrocarbon. The second formation that deposited a source rock is Karper formation. Geochemistry measurement showed that generally source rock in this formation is potential to produce gas than oil.

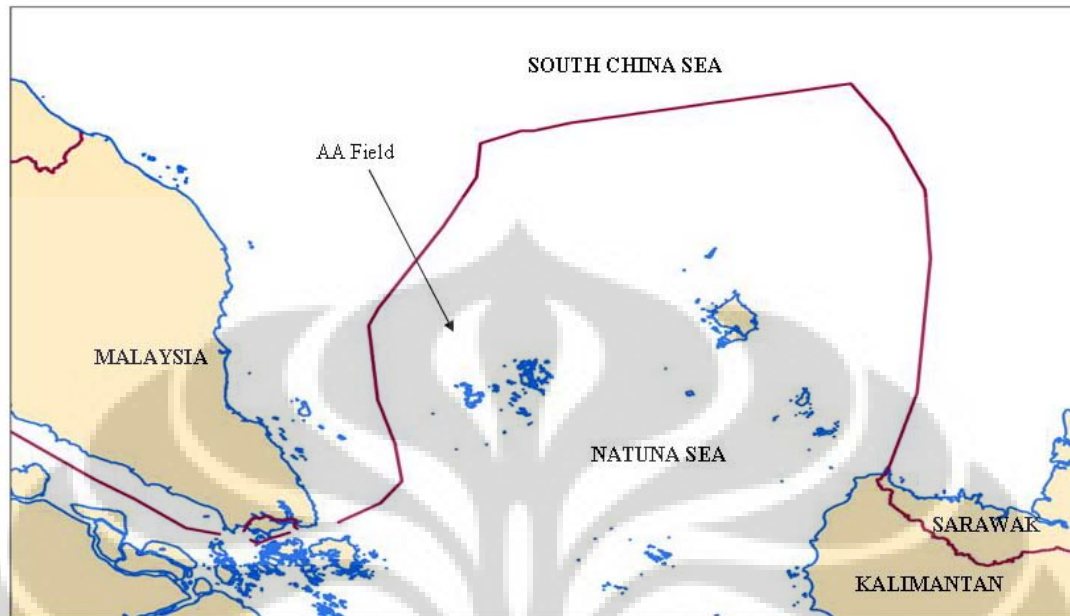


Figure-1.1: Location of AA field, West Natuna, Indonesia.

1.3.2.2. Migration

Primary migration is the first phase of the migration process; it involves expulsion of hydrocarbons from their fine-grained, low permeability source rock into a carrier bed having much greater permeability. Secondary migration is the movement of oil and gas within this carrier bed. Migration initiated in Miocene until Pleistocene. Berendson in 1991 revealed that oil had started to migrate from Paus formation since Late Miocene with relative vertical trend.

1.3.2.3. Reservoir Rock

In AA field, Cakalang formation has good quality reservoir. The formation was deposited in the post rift section. This section was deposited as the extensional tectonic regime ceased. This makes the overall thickness of the interval relatively

constant. Many of reservoirs were discovered in this formation. This makes Cakalang formation becomes a main target of exploration in AA field.

1.3.2.4. Trap

Generation of thrust fault due to an inversion produced an anticline. This anticline becomes a trap in the AA field. In West Natuna Basin, there are 3 types of trap, structural, stratigraphic, and combination between structural and stratigraphic. Structural type is associated with forms of anticline. Meanwhile, stratigraphic trap is associated with reservoir stacked forms on channel.

1.3.2.5. Seal

Seal in AA field is located in Karper formation. Sediment in this formation was deposited in lake environment and had a main lithology of shale. The Karper shale is extensively deposited over the entire area, and provides regional shale for underlying reservoirs in almost Block PSC area.

CHAPTER II DATA AND METHODOLOGY

2.1. Data

2.1.1. Log Data

The well logs data used in the AA field study were V_P , V_S , Density, Porosity, Water Saturation, V_{shale} , V_{clay} , Gamma Ray and Resistivity. The wells are located at the following inline and xline:

Well Name	Inline	Xline
AA-2	6575	4398
AA-3	6835	4210
AA-4	6870	4530

2.1.2. Seismic Data

The seismic 3D volume used in the thesis is near angle stack with the following information:

Inline : 6500 - 7500, increment 1, a total of 201 inlines at a spacing 12.5 m.

Xline : 4100 - 4600, increment 5, a total of 501 xlines at a spacing 12.5 m.

Time range : 0 – 2500 msec.

The study area of seismic 3D of AA field can be shown below:

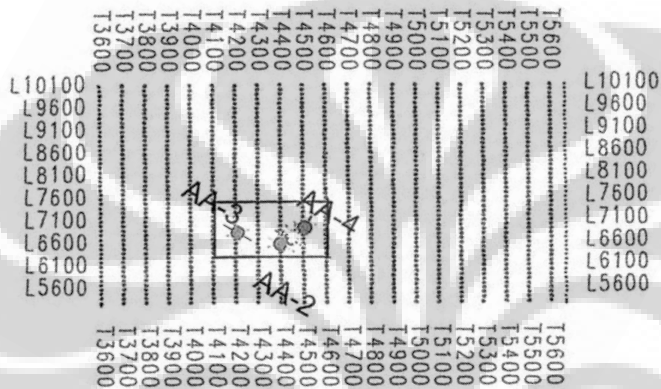


Figure- 2.1: Basemap of AA field.

2.2. Methodology

The thesis consists of the following work:

2.2.1. Well data

1. Doing fluid replacement logs on V_p , V_s , ρ_b with S_w variation.
2. Creating an elastic logs of insitu case, hydrocarbon case and wet case (AI, PR).

3. Creating cross plots of elastic properties.

2.2.2. Well Log to Seismic Tie:

1. Wavelet extraction.
2. Creating 1D synthetic.
3. Creating 2D synthetic.

2.2.3. AVO Inversion:

1. Creating AI, PR, volumes.
2. Creating cross plots of amplitude Z_p and PR.

The study can be grouped into AVO Modeling and AVO Inversion as shown on flowchart in FIGURE-1.4. In AVO Modeling we do many cross plots based on logs data to find the best cross plots which can discriminate lithology and fluids. While in AVO Inversion we use seismic angle stack to see reservoir direction or hydrocarbon indication by extracting lithology and fluids information from seismic data.

2.3. Scope of Study

The scope of this study is limited to AVO Inversion to derive elastic parameter. The elastic parameter will be used as lithology and fluid discriminator. The final output will be lateral section of direct hydrocarbon indicator, acoustic impedance (AI) and poisson ratio (PR).

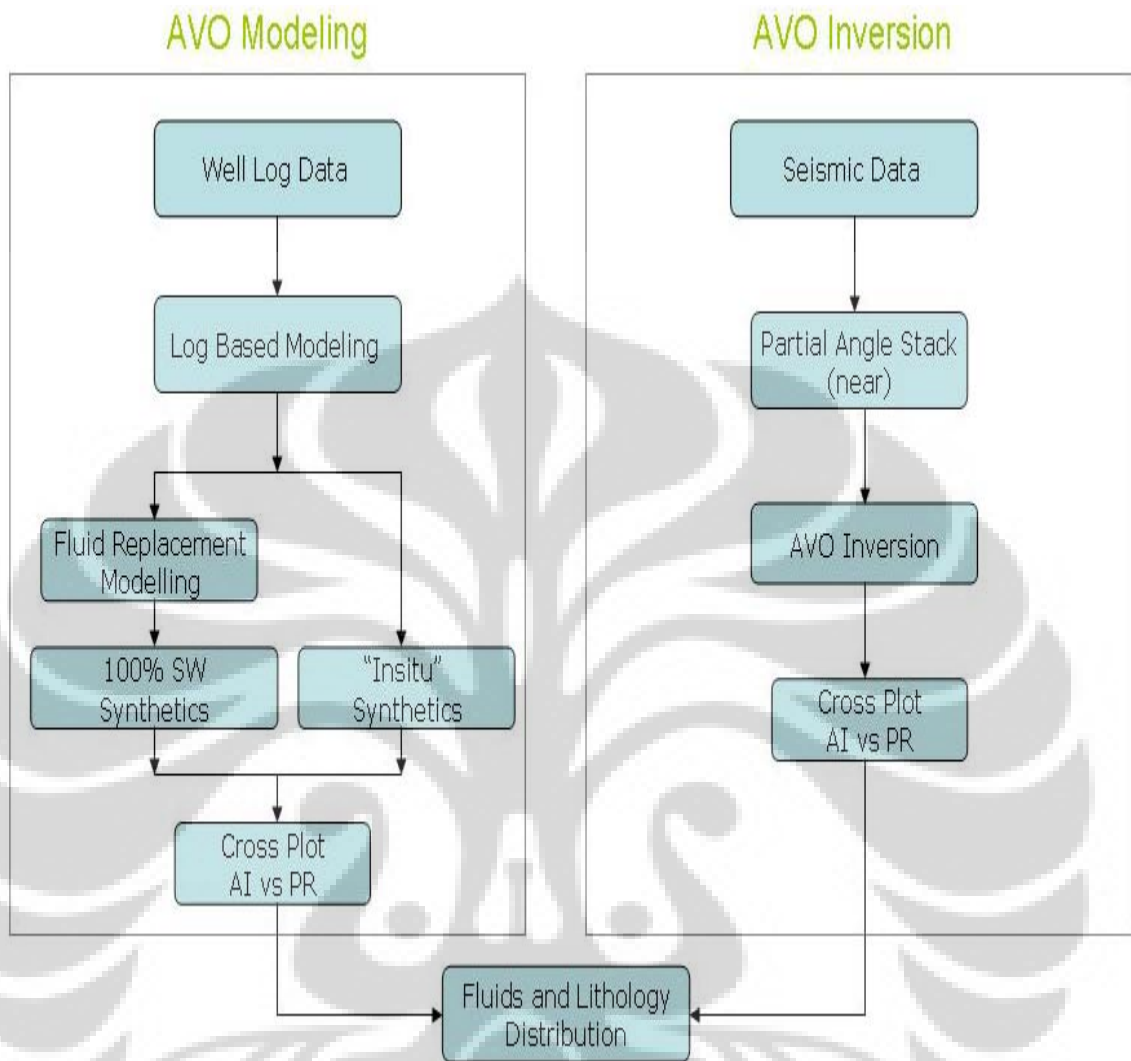


Figure-2.2: Flowchart of Fluids and Lithology Prediction Through AVO Inversion, a Case Study in the AA Field, West Natuna Basin, Indonesia.

CHAPTER III

THEORY

Several techniques allow us to extract lithology information from seismic data. However to be able to discuss the seismic method available for the prediction of lithology, we must first discuss these lithologic parameters themselves, i.e. what is a rock and how do seismic measurements tell us about it.

The pioneers for behavior of seismic waves as they pass through porous, fluid-filled sedimentary rock was Gassmann (1951), who used elastic theory to predict the interrelationships among the various rock parameters and Biot (1951), who was the first to look at the theory of the propagation of waves through a fluid-filled medium. Recently, Hilterman has made the results better known and has restated a practical method for solving the problem of P and S-wave velocity (and hence Poisson ratio) as a function of water saturation and porosity.

In this chapter we will first discuss the basic concepts of lithologic properties of density, bulk modulus, shear modulus and velocity. The discussion will conclude with various theoretical relationships in porous media, such as Biot Gassmann and Castagna. We will then discuss the theory of AVO analysis, modeling and inversion.

3.1. Rock Physics

The rock physical properties can be used to describe the rock condition of reservoir. The rock physical properties consist of density, P-wave velocity, S-wave velocity, Bulk Modulus, Shear Modulus and Poisson Ratio. Every property has its own characteristic.

3.1.1. Density

Density is simply mass per unit volume. In other words, the heavier the rock sample, the higher its density. In general the density is related to a number of factors, as shown in Figure-3.1.

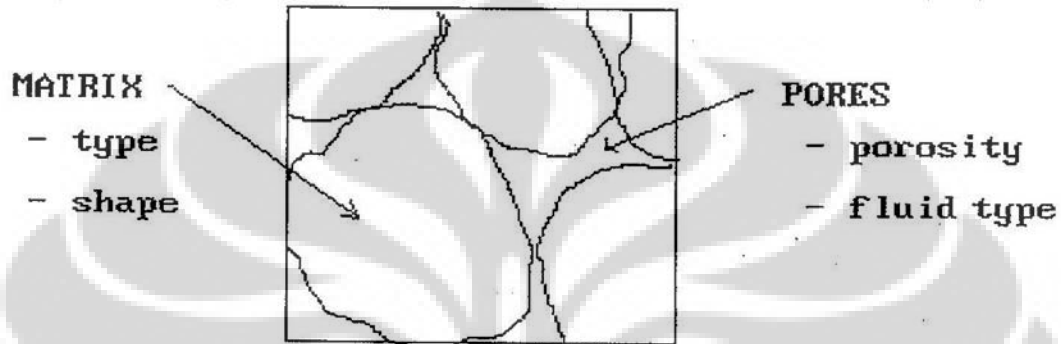


Figure-3.1: Rock properties are determined by matrix type, porosity, and fluid type.

If we assume that there is a single mineral type, or that we know the average density of the overall rock matrix, and that there is a single fluid filling the pores, Wyllie's equation can be used to determine the density, written as:

$$\rho_b = \rho_m (1-\emptyset) + \rho_f \emptyset \quad (3.1)$$

where ρ_b = bulk density of the rock,

ρ_m = density of the rock matrix,

ρ_f = density of the rock fluid,

\emptyset = porosity of the rock.

If we assume that the fluid is a mixture of several other fluids, specifically water and hydrocarbon, the fluid density is given by

$$\rho_f = \rho_w S_w + \rho_{hc} (1-S_w) \quad (3.2)$$

where S_w = water saturation

ρ_w = density of water (close to 1 g/cm³),

and ρ_{hc} = density of hydrocarbon.

Obviously, we could combine equations 1 and 2 into the single equation shown as:

$$\rho_b = \rho_m (1-\phi) + \rho_w S_w \phi + \rho_{hc} (1-S_w) \phi \quad (3.3)$$

Figure-3.2 is a plot of density versus water saturation in both a gas reservoir and an oil reservoir with a porosity of 25%.

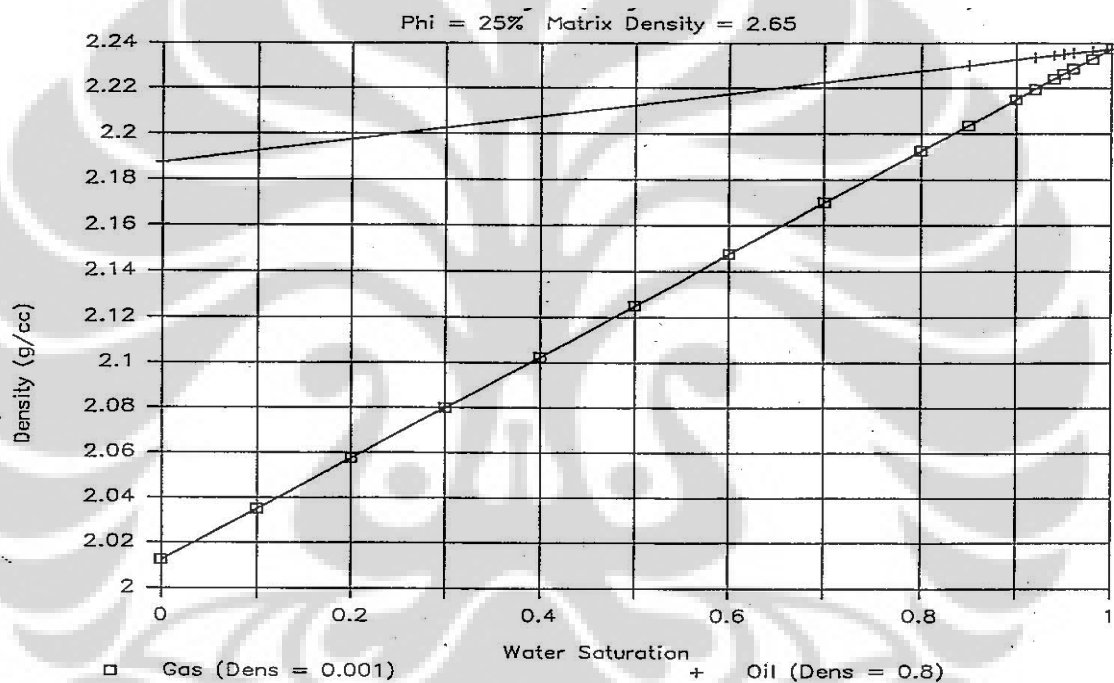


Figure-3.2: Wylli's equation applied to an oil and gas reservoir.

In Figure-3.2, density drops much more rapidly in a gas reservoir than an oil reservoir. Density enters into the equations of such other parameters as compressional and shear wave velocities, and acoustic impedance, all of which effect the response of seismic wave to the subsurface. The dramatic difference seen in the density of gas and oil filled reservoirs will therefore play an important role in the seismic interpretation of these reservoirs.

3.1.2. Velocity

There are two types of wave when analyzing seismic data, the compressional (P-wave) and the transverse (S-wave). The equation for both of these waves can be written:

$$V = (M/\rho)^{1/2} \quad (3.4)$$

Where M = elastic modulus

ρ = density

There are three ways in which a rock can be deformed: by pushing from above (compression), by pulling from above (tension), or by pushing from the side (shear). In both tension and compression, the volume (or in the case shown, the area) of the rock changes, but its shape does not. In the case of a shear deformation, the shape of the rock has changed but its volume has not.

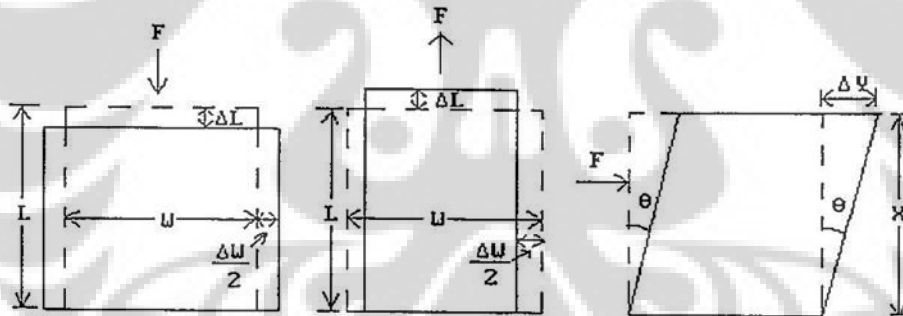


Figure-3.3: A rock may be deformed by (a) compression, (b) tension, and (c) shear, where F = force applied.

Figure-3.3 also illustrates the concepts of stress and strain. The force per unit area required to produce a deformation is called stress. The deformation resulting from a stress is called a strain. The figure shows three types of strains, two related to a compressive or tensile stress, and one related to a shear stress. These are:

$$\text{Longitudinal strain: } e_L = \Delta L/L \quad (3.5)$$

$$\text{Transverse strain : } e_w = \Delta L/L \quad (3.6)$$

$$\text{Shear strain : } e_s = \Delta Y/X = \tan \emptyset \quad (3.7)$$

Figure-3.3 shows only a two dimensional cross section of a rock cube. A complete description of strain involves the three dimensional cube of a rock itself, and its termed volumetric strain. This is illustrated in Figure-3.4, which show a cubicle volume before and after a stress. In this case, the strain is written:

$$\emptyset = \Delta V/V \quad (3.8)$$

where \emptyset = volumetric strain

ΔV = change in volume

V = initial volume

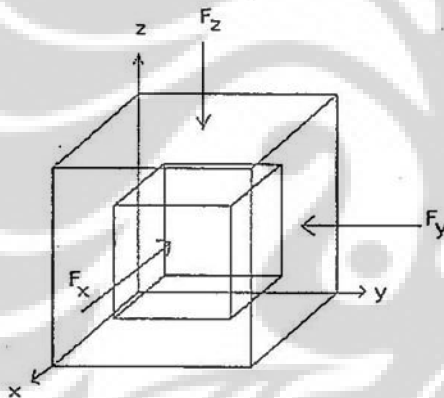


Figure-3.4: Volumetric stress or cubicle dilatation.

Stress is given as force per unit area, and this can be written as:

$$P = F/A \quad (3.9)$$

Where P = stress,

F = force,

A = area.

In perfectly elastic medium, stress and strain can be related to each other by Hooke's Law, which states that:

$$\text{STRESS} = \text{CONSTANT} \times \text{STRAIN} \quad (3.10)$$

Strain is non dimensional, since it simply describes the proportional deformation of a material. The constant that relates stress and strain (which was introduced in equation 10) is called the modulus and has the same units as stress (force over area, or dynes/cm²).

For a purely longitudinal strain, the modulus is called Young's modulus and the stress/strain relationship can be written:

$$PL = E \Delta L/L \quad (3.11)$$

Where E is Young's modulus

For a shear strain, the modulus is called the shear modulus, or the rigidity, and can be written:

$$P_s = \mu e_s \quad (3.12)$$

Where P_s = shear stress,

μ = shear modulus,

e_s = shear strain.

For a volumetric strain the constant is called the bulk modulus, or incompressibility. In symbols:

$$P_H = k \Delta V/V \quad (3.13)$$

Where P_H = Hydrostatic stress,

$\Delta V/V$ = volumetric strain or dilatation,

k = bulk modulus which is the inverse of compressibility ($k = 1/C$) (3.14)

P wave velocity may be written:

$$V_p = \left[\frac{K + 4/3 \mu}{\rho} \right]^{1/2} \quad (3.15)$$

where $M = k + 4/3 \mu$.

For S wave, the equation is written:

$$V_s = (\mu/\rho)^{1/2} \quad (3.16)$$

Where $M = \mu$ = the shear modulus.

An important diagnostic in seismic lithologic determination is the ratio of P-wave velocity to S-wave velocity. We can derive from the preceding equations that

$$(V_P/V_S)^2 = k/\mu = 4/3 \quad (3.17)$$

Another important parameter is the Poisson's ratio, which can be given in terms of V_P to V_S ratio:

$$\sigma = \frac{r^2 - 2}{2(r^2 - 1)} \quad (3.18)$$

Where σ = Poisson's ratio, and

$$r = V_P/V_S$$

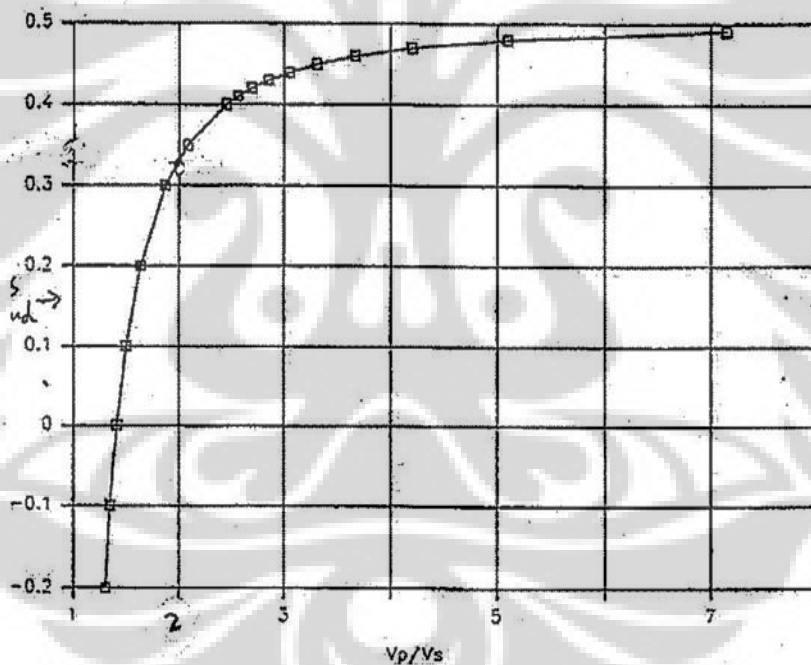


Figure-3.5: Poisson's ratio as a function of P-wave to S-wave ratio.

The key parameters needed for seismic lithology i.e., density, P-wave, S-wave, velocity, as well as the elastic constants: incompressibility, rigidity and Poisson ratio.

Again, the most straightforward relationship between porosity and velocity is given by the Wyllie time-average formula where:

$$1/V_b = (1-\Phi)/V_m + S_w\Phi/V_w + (1-S_w)\Phi/V_{hc} \quad (3.19)$$

Where V_b = bulk density

V_{hc} = velocity of hydrocarbon,

V_m = matrix velocity,

V_w = water velocity.

A plot of Wyllie's equation for both a porous gas sand and a porous oil sand of differing water saturation is given in Figure-3.6.

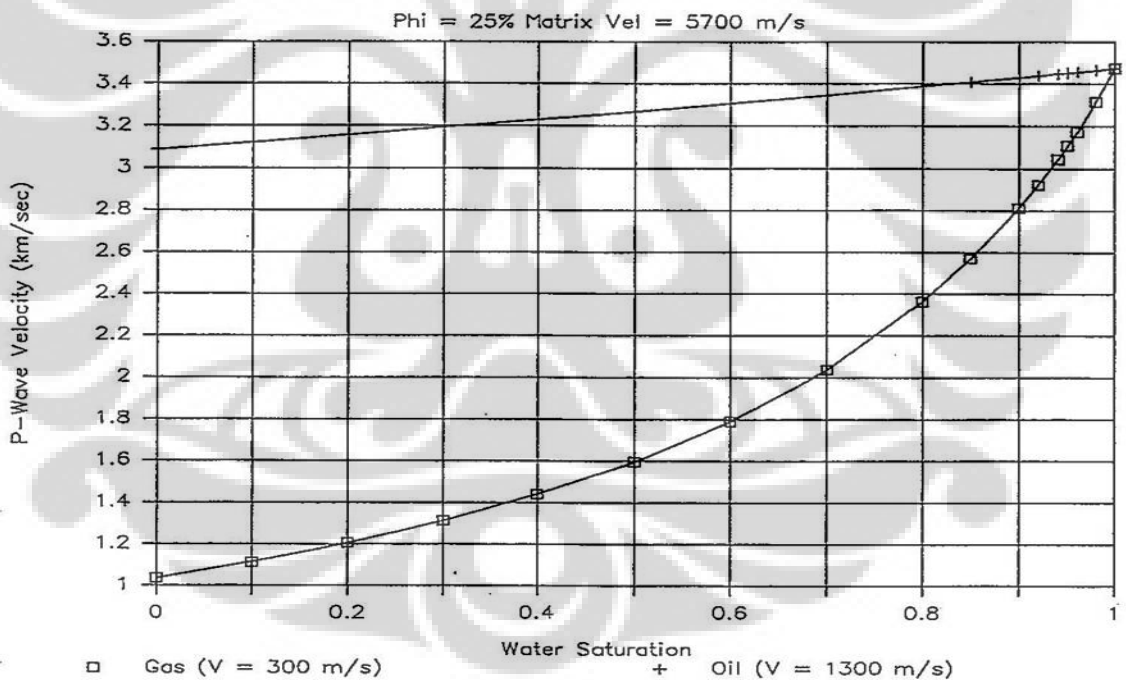


Figure-3.6: P-wave velocity vs Water Saturation for both a gas sand and an oil sand.

3.1.3. The Biot Gassmann Model

The time average velocity works well for fluid saturated sediment at depth. However, it does not appear to correct predict the effects seen in shallow, gas saturated sand.

To derive P-wave velocity as a function of water saturation from the time average equation in a gas reservoir, let us see the curve of Poisson ratio versus P-wave velocity as shown in FIGURE-3.17 which displays a gradual decrease in velocity. However experimental results show a dramatic dip in velocity as soon as any gas introduced. Geertsma quantified this effect with the following equation which is extended of equation (3.15) and expression for P-wave velocity in a non porous rock.

$$V_P = \left((k_b + 4/3 \mu_b + \frac{(1 - k_b/k_s)^2}{(1-\phi - k_b/k_s)/k_s + \phi/k_f}) / \rho_b \right)^{1/2} \quad (3.20)$$

Where V_P = P-wave velocity

k = bulk modulus

μ = shear modulus

ρ = density

b, s, f = average, solid and fluid components.

The third term of the above equation is a fluid term, which goes to zero if the ratio k_b/K_s is equal to 1. In equation (3.20), only ρ_b and K_f will vary as a function of water saturation. Density can be computed using equation (3.3). For the fluid in the pores, the relationship is identical to that for density, except the incompressibility is inverted:

$$1/k_f = S_w/k_w + (1-S_w)/k_{hc} \quad (3.21)$$

In equation (3.20), k_s , k_w and k_{hc} are all empirically derived valued while k_b and μ_b can be measured by either measuring V_P and V_S from a test sample, or by assuming the Poisson ratio's of a gas filled rock sample.

The result of Biot Gassmann analysis are shown in Figure-3.7 for a gas sand of porosity 33%. Clearly there is a more sudden drop in P-wave velocity than obtained

using the time average equation. It is noted that this equation is extremely important for shallow gas sands.

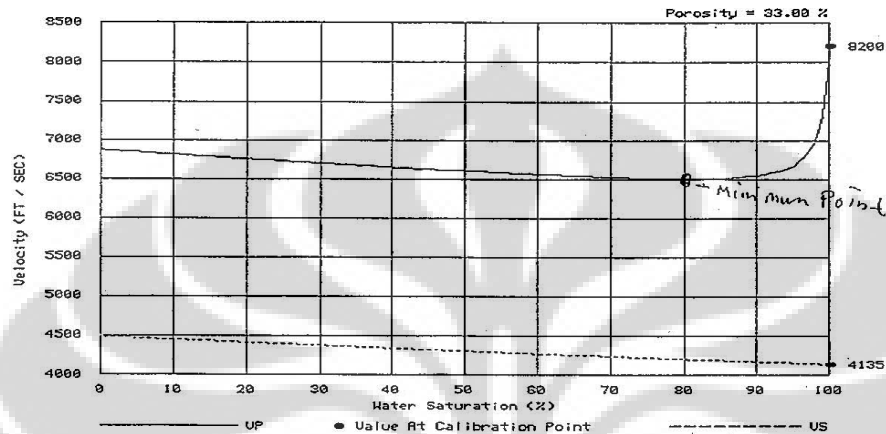
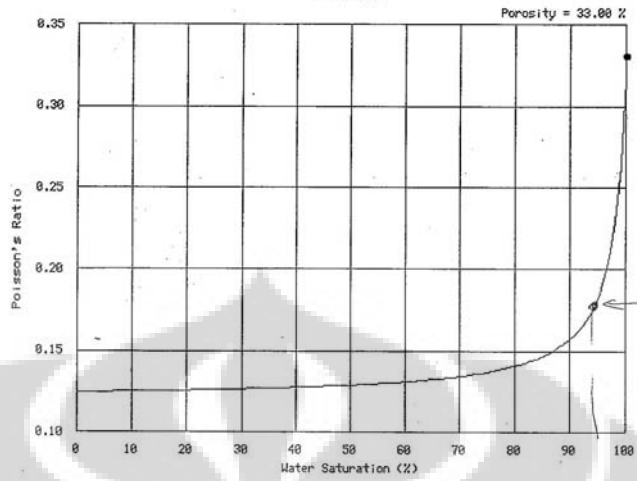


Figure-3.7: A Biot Gassmann plot of P-wave and S-wave velocity versus water saturation in a gas sand using the Biot Gassmann equation (Gulf Coast and – Gas Filled).

The above figure also shows the S-wave velocity as a function of water saturation and shows there is not sudden change in S-wave velocity, only a gradual rise. This is due to only P-wave velocity is affected by bulk modulus, and the shear modulus is constant., leaving S-wave velocity to be influenced only by density.

The effect is also illustrated in Figure-3.8, where Poisson ratio is plotted against water saturation. While Figure-3.9 and Figure-3.10 shown a case of an oil filled reservoir, which shown that there is much less of an effect on the P-wave velocity and the Poisson's ratio in an oil reservoir than in a gas reservoir.



◦ value at calibration point

Figure-3.8: A Biot Gassmann plot of Poisson's ratio versus water saturation in a gas sand (Gulf Coast Sand – Gas Filled).

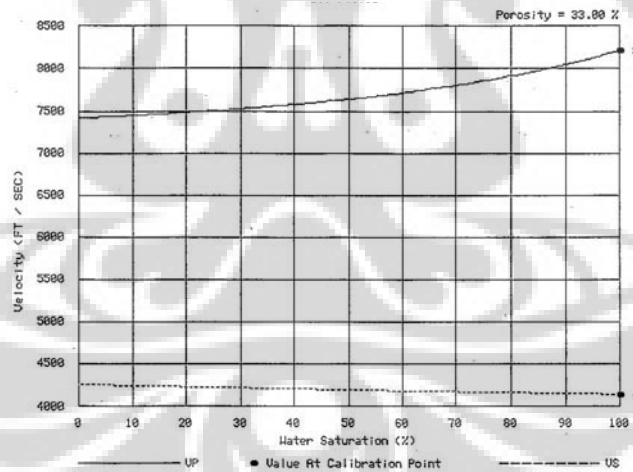


Figure-3.9: A Biot Gassmann plot of P-wave and S-wave velocity of a function of water saturation in an oil filled sand (Gulf Coast Sand – Oil Filled).

We have discussed a number of variables: P-wave velocity, S-wave velocity, Poisson's ratio, and water saturation. Another useful plot is that of Poisson's ratio

versus P-wave velocity with water saturation values plotted for a constant porosity (33%) was shown In Figure-3.10.

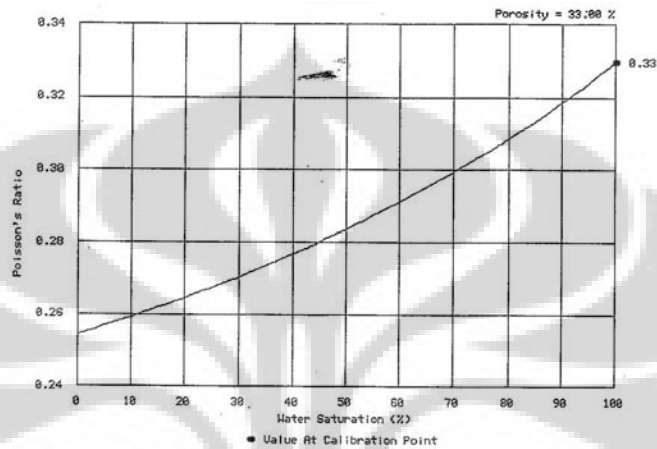


Figure-3.10: A Biot Gassmann plot of Poisson's ratio as a function of water saturation on an oil filled sand (Gulf Coast Sand – Oil Filled).

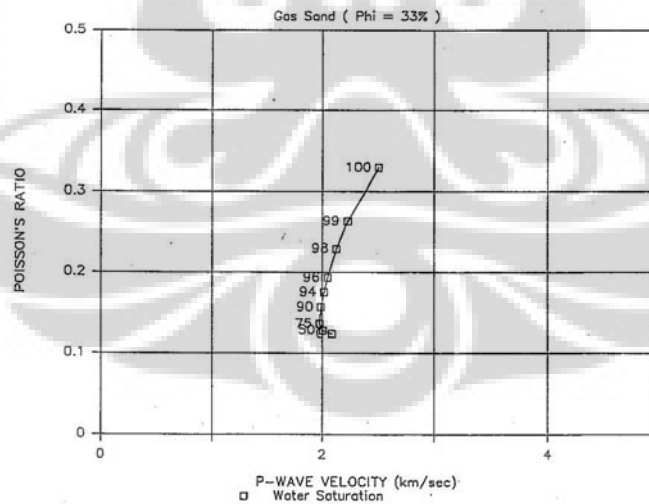


Figure-3.11: P-wave velocity versus Poisson's ratio plot for a number of different water saturations.

3.1.4. Relationship Between P and S Velocities (Castagna's Relationship)

The Biot Gassmann model is mathematically complex and the theory falls down when applied to small grained clastic rocks, such as mudstones. In this case, Castagna et al (1985) derived a much simpler empirical relationship between P-wave and S-wave velocity, which can be written:

$$V_p = 1.16 V_s + 1.36 \quad (3.22)$$

Where velocity is in km/sec.

This is simply the equation for a straight line. A plot of this line, and the observations that fit it from previous work, is given in Figure-3.12. This line is also called the mudrock line.

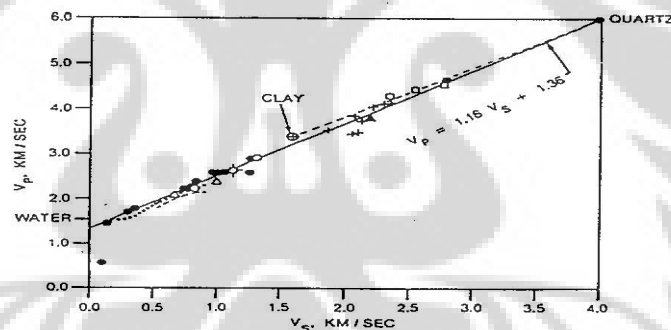


Figure-3.12: The mudrock line.

We will consider two plots: Poisson's ratio versus P-wave velocity and V_p/V_s ratio versus P-wave velocity as shown in Figure-3.13 and Figure-3.14. Notice that the plot of Poisson's ratio against P-wave velocity (in Figure-3.13) shows that the lowest Poisson's ratio is 0.1. On the V_p/V_s ratio against P-wave velocity (in Figure-3.14) the curve approaches the value 1.5 asymptotically. These values ($\sigma = 0.1$ and $V_p/V_s = 1.5$) represent the so called "dry rock" value for dry, porous sandstone. Thus, the "mudrock" line approaches the "dry rock" lines at the P-wave velocity increases.

Finally, Castagna also shows that Gassmann's equations predict velocities that fall approximately on the mudrock line in the water-saturated case.

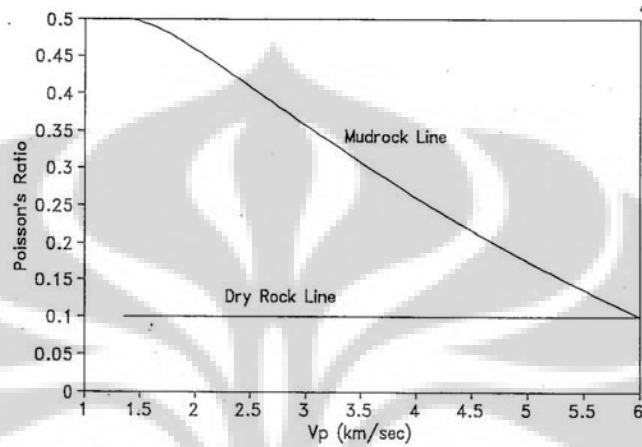


Figure-3.13: Poisson's Ratio versus P-wave Velocity.

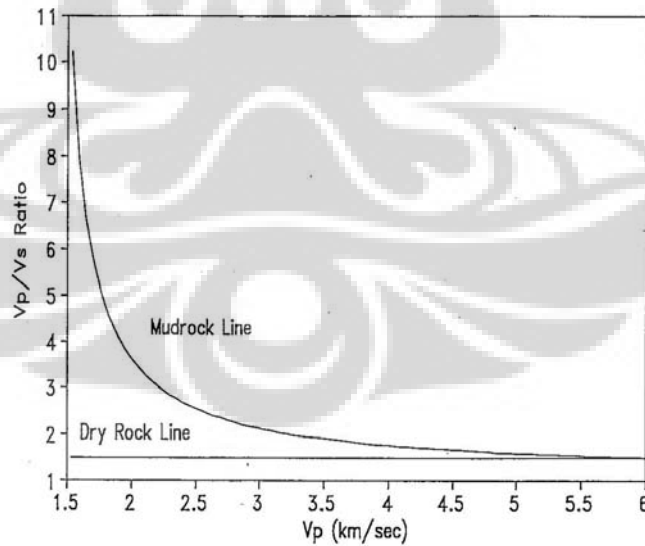


Figure-3.14: V_p / V_s Ratio versus P-wave Velocity.

3.2. AVO in Reservoir Characterization

AVO has a great role in reservoir characterization especially to identify the fluid content in a reservoir. Change of amplitude is affected by offset and Poisson's Ratio. The change of Poisson's Ratio depends on the change of fluid content in the layer. Rutherford and Williams divided 3 class of sandstone : Class 1 High Impedance Gas Sand, Class 2 Near Zero Impedance Gas Sand, and Class 3 Low Impedance Gas Sand. In 1998, Castagna revealed the Class 4. The difference of all class is shown below:

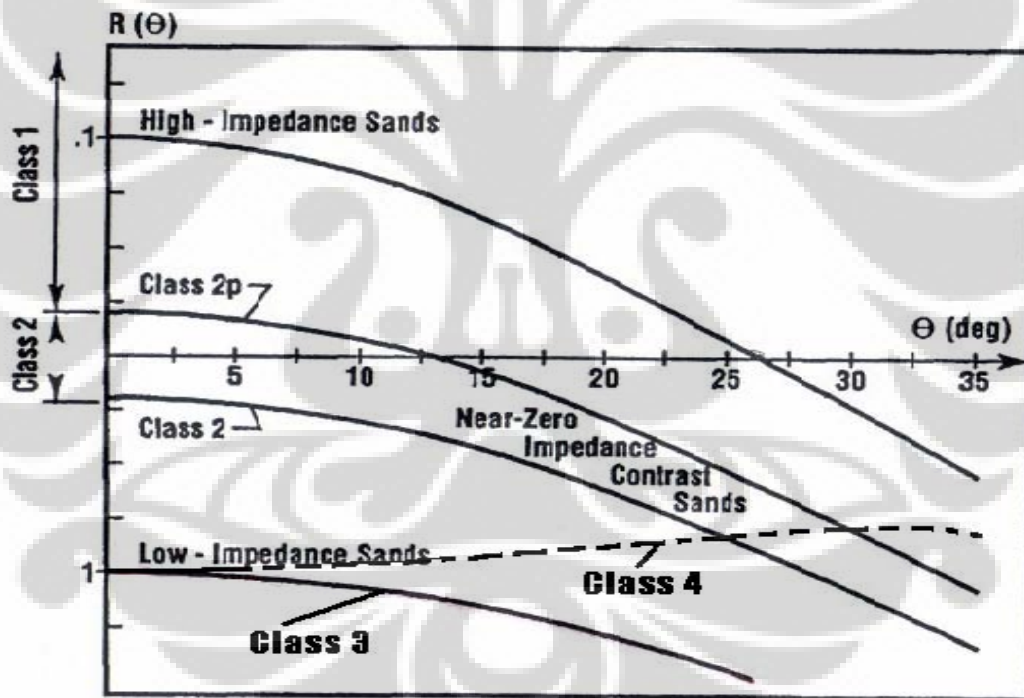


Figure-3.15: Plot of Reflection Coefficient to Incident Angel in top of gas sand by Rutherford and Williams.

3.2.1. Class 1: High Impedance Gas Sand

Sandstone class 1 has relatively high impedance than its seal layer, which usually is shale. Interface between shale and this sandstone will result high positive coefficient reflection. The top curve on figure 2.5 showing anomaly for sandstone class 1, usually this sandstone is found in coastal exploration area. This sandstone is mature sandstone which has moderately to highly compacted. Coefficient reflection of high acoustic impedance sandstone is positive on zero offset and began with amplitude magnitude decreased as the offset increases.

Magnitude of amplitude change to offset (usually known as the term 'gradient') for sandstone class 1 usually bigger than gradient of sandstone class 2 or 3. Reflectivity magnitude of sandstone class 1 initially will decrease as the offset increasing and may have polarity change on certain angle and then the amplitude increase will happened again as the offset increases with the oppositely polarity of the initial polarity.

3.2.2. Class 2: Near Zero Impedance Contrast Sand

Sandstone class 2 has almost the same acoustic impedance as the seal rock. This sandstone is a compacted and moderately consolidated sandstone. Gradient of sandstone class 2 usually has big magnitude, but generally it's smaller than the magnitude of sandstone class 1. Reflectivity of sandstone class 2 on small offset is zero. This is often blurred due to the presence of noise on our data seismic. The reflectivity suddenly emerged on bigger offset that is when the reflection amplitude is located on a higher level than noise.

Polarity change happens if the reflection coefficient is positive, but usually it's undetected, because it happens on the near offset where the signal level is under the noise.

Sandstone class 2 might and might not be related to amplitude anomaly on stack data.

If the angular range is available, so the amplitude will rise as the offset increasing, it is amplitude anomaly on stacked data.

3.2.3. Class 3: Low Impedance Gas Sand

Sandstone class 3 has lower acoustic impedance than the seal rock. Usually this sandstone is the less compacted and unconsolidated sandstone. On seismic data, sandstone class 3 has big amplitude anomaly and reflectivity in the whole offset. Usually the gradient is significant enough but it has lower magnitude than the sandstone class land 2 during RC's normal incidence angle is always negative. In some additions, relatively small change of amplitude to offset can cause detection difficulties because the presence of tuning thickness, attenuation, recording array, and decreasing of signal to noise ratio. Sandstone class 3 sometime has high amplitude response which relatively flat along with the offset as shown in Figure-3.16.

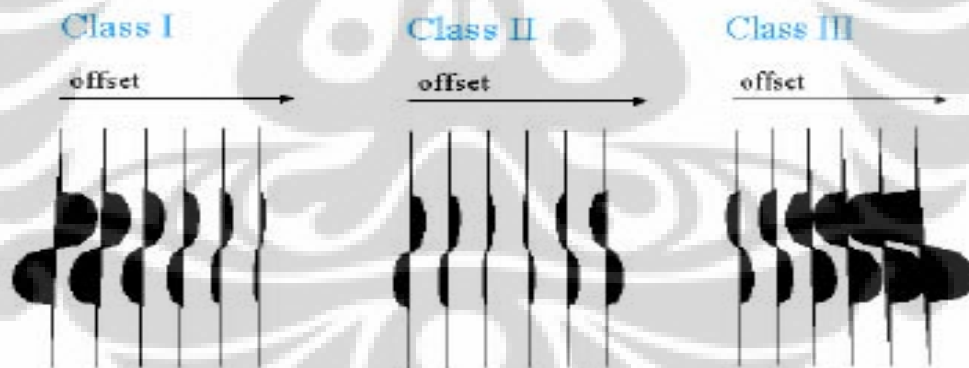


Figure-3.16: Amplitude to offset – Rutherford and Wiliam classification (1985).

3.2.4. Class 4 Anomaly

In fact, the forth class of gas sandstone is the anomaly with the reflection coefficient

becoming positive along as offset increases, but the magnitude decreased as the offset increases. Sandstone class 4 often emerged when the porous sandstone, which is restricted by the lithology, has high seismic wave velocity, such as hard shale, siltstone, tightly cemented sand, or carbonate. Sandstone class 4 is the bright spot, but the reflection coefficient decreased as the offset increases.

Class	Relative Impedance	Quadrant	A	B	Amplitude vs. Offset
I	Higher than overlying unit	IV	+	-	Decreases
II	About the same as the overlying unit	II, III, or IV	+ or -	-	Increase or decrease; may change sign
III	Lower than overlying unit	III	-	-	Increases
IV	Lower than overlying unit	II	-	+	Decreases

Figure-3.17: Reflektion coefficient of gas sandstone againts the offset for 4 classes of AVO anomaly.

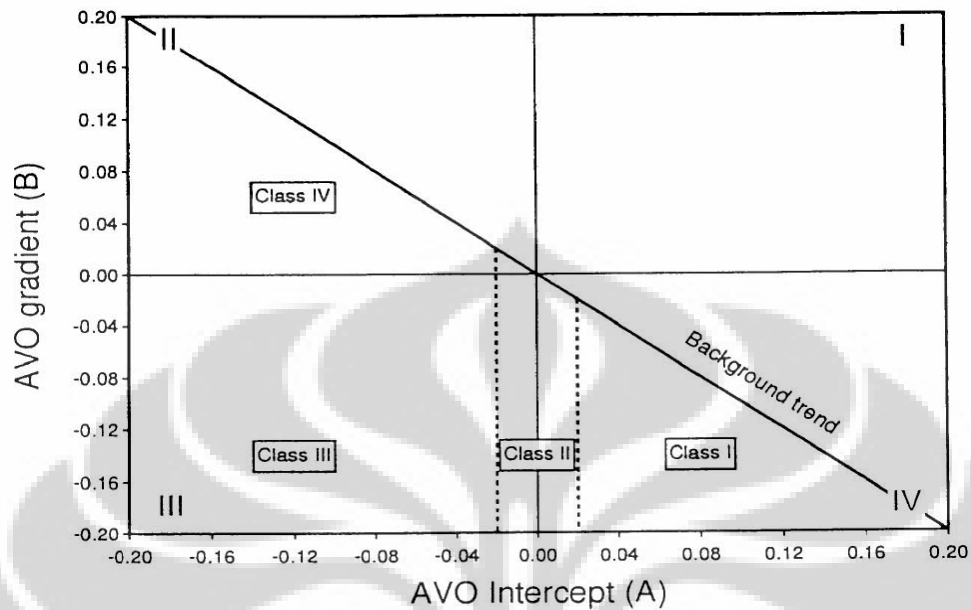


Figure-3.18: Crossplot of AVO intercept against gradient shows 4 possibilities of quadrant.

3.3. Acoustic Impedance and Reflectivity

If the seismic waves strikes the boundary between the media at an angle greater than zero with the vertical, it is possible for the reflection to have an amplitude of zero even if there is an acoustic impedance change. The nature of acoustic impedance:

$$Z = \rho V_P \quad (3.23)$$

Where Z = acoustic impedance

ρ = density

V_P = P-wave velocity

The product of impedance times velocity gives the modulus:

$$ZV = \rho V^2 = \rho (M/\rho) = M \quad (3.24)$$

Equation 3.24 is general, and holds equally well for both P and S waves, the modulus M can be either bulk or shear modulus.

Thus, the acoustic impedance of a rock, like the modulus, is a fundamental property of a rock which determines its response to deformation.

For the case of seismic waves which strike the interface at an angle of zero, the reflection coefficient is simple:

$$R = \frac{Z_2 - Z_1}{Z_2 + Z_1} \quad (3.25)$$

Where Z_1 = acoustic impedance of layer above boundary

Z_2 = acoustic impedance of layer below boundary

R = reflection coefficient

Although equation 3.25 is normally interpreted to be the result of zero incident P-waves, it could equally well represent the reflection due to zero incidence S-waves. In that case, S-waves velocity would be substituted for P-wave velocity in equation 3.23.

CHAPTER IV

RESULT AND DISCUSSION

This chapter summarizes the AVO modeling, AVO analysis and AVO inversion study of the AA field at West Natuna Basin. The study was conducted using 3D volume of partial angle stack (near). A migrated partial stack section was connecting the wells AA-2, AA-3 and AA-4 were extracted from the 3D volume for input to acoustic impedance inversion. Log data from 3 wells, AA-2, AA-3 and AA-4 were used to extract seismic wavelet, construct the reservoir fluid model used to generate synthetic seismic gathers and for the inversion initial model.

4.1. Petrophysical Analysis

The objective of this step is to investigate whether shale, tight sand and good porosity sand can be separated and to observe if gas, oil and water can be discriminated. The analysis creates the cross plots of insitu case (before fluid replacement). Many cross plots have been generated but only the best cross plots will be shown.

A through rock physics analysis is necessary to determine if this technique may be viable given the geologic setting, and the quality of available seismic and borehole log data. By cross plotting various rock properties obtained from the well logs, we are able to observe the separation or clustering of data according to lithology and/or fluid saturant. Borehole data from AA field shows distinct separation between brine and hydrocarbon (gas and oil) saturated lithology using P-impedance versus Poisson Ratio cross plot as shown in Figure-4.1 to Figure-4.3.

These results imply that there is strong possibility that pore fluids and, to a lesser extent, lithology can be detected and differentiated from seismic data and may begin to predict what the nature of anticipated seismic AVO response.

In general, petrophysical analysis facilitates a greater understanding of the field and attributes of the rock that drive the seismic response.

From Figure-4.1 to Figure-4.3, it is known that good porosity sand of AA-2, AA-3 and AA-4 can be separated from shale and tight sand by using 'P-Impedance versus Poisson's Ratio versus Porosity' cross plots. The gas bearing sand at AA-2 has P-impedance < 19000 (ft/sec*gr/cc), the oil bearing sand at AA-3 has P-impedance between 19000 (ft/sec*gr/cc) and 21600 (ft/sec*gr/cc), and oil-water bearing sand at AA-4 has P-impedance > 21600 (ft/sec*gr/cc). Figure-4.4 and Figure-4.5 show that oil can be separated from water by Poisson's Ratio about 0.275 at AA-4 well.

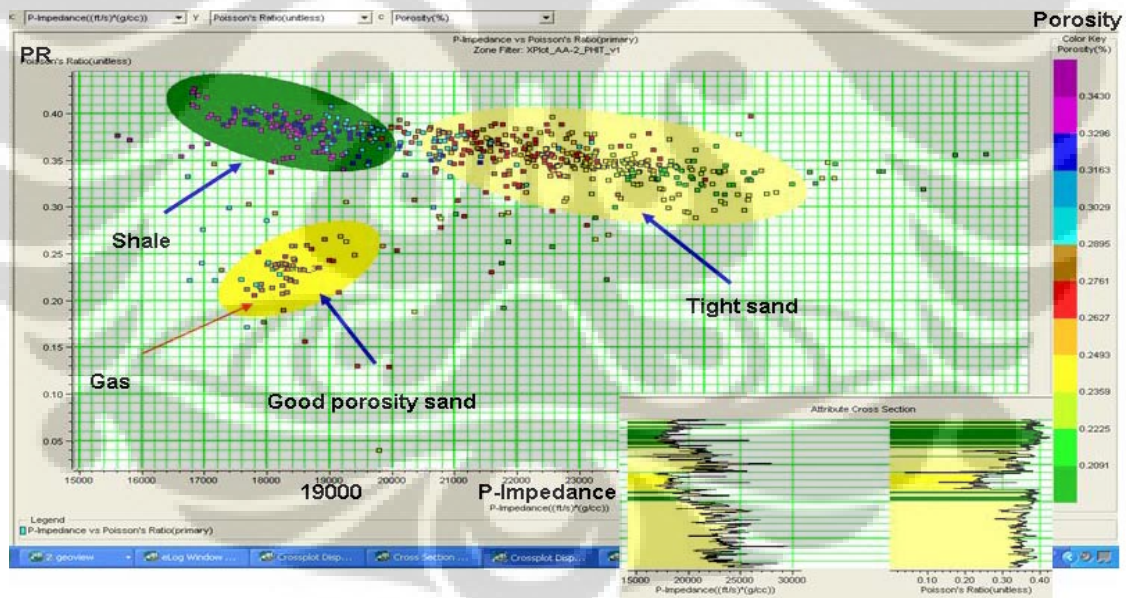


Figure-4.1: P-impedance versus Poisson's Ratio versus Porosity of AA-2.

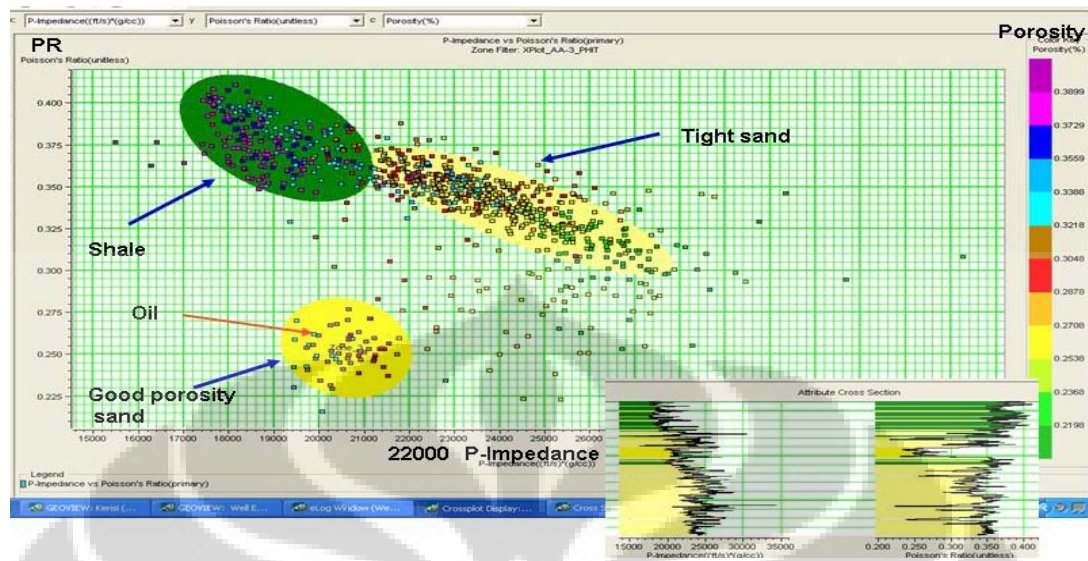


Figure-4.2: P-impedance versus Poisson's Ratio versus Porosity of AA-3.

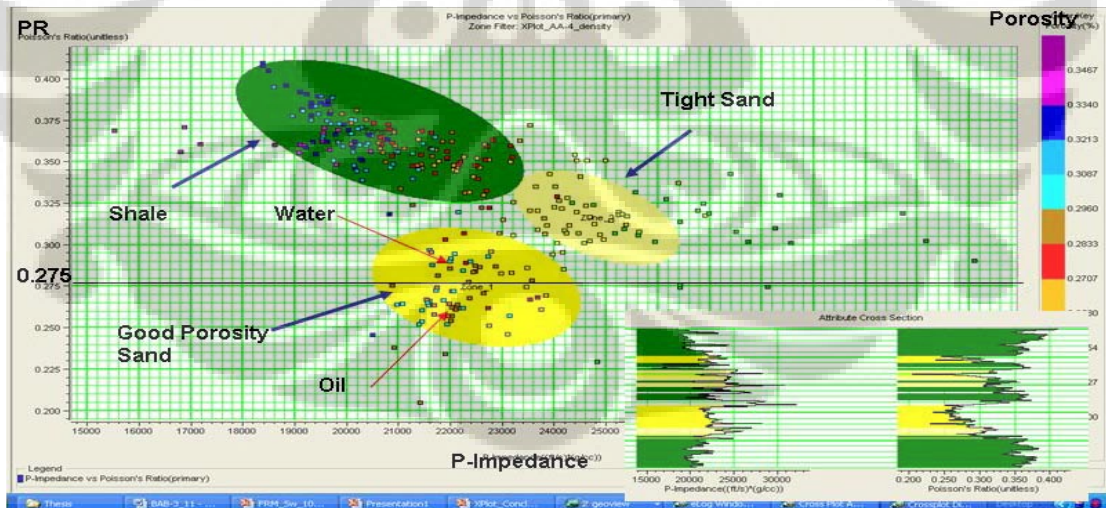


Figure-4.3: P-impedance versus Poisson's Ratio versus Porosity of AA-4.

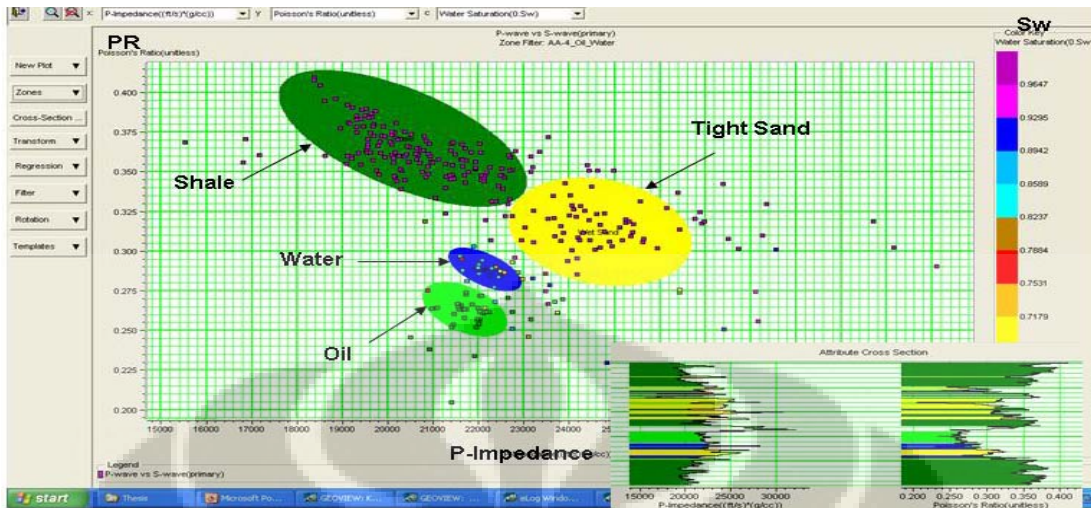


Figure-4.4: P-impedance versus Poisson's Ratio versus Water Saturation of AA-4.

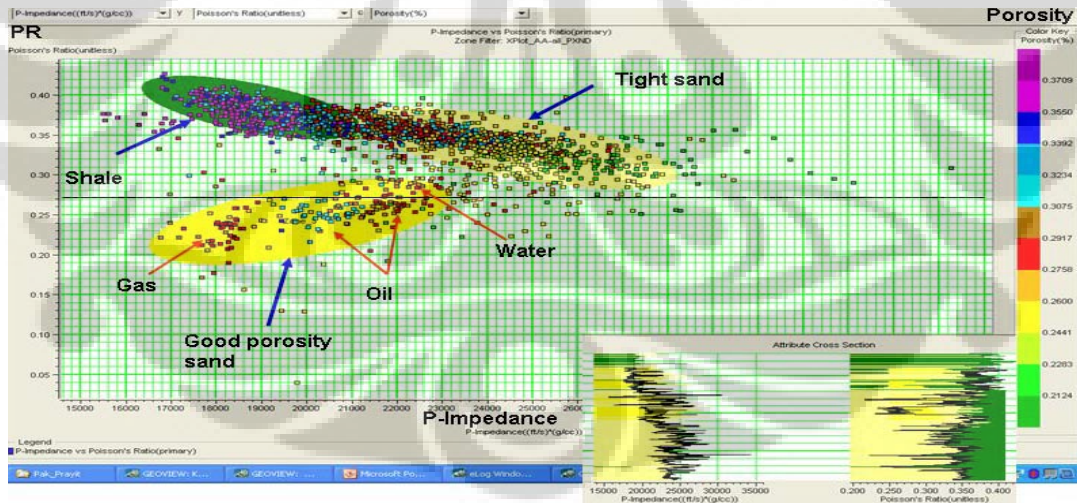


Figure-4.5: P-impedance versus Poisson's Ratio versus Porosity of AA-2, AA-3 and AA-4.

Figure 4.5 is a ‘P-impedance versus Poisson’s Ratio versus Porosity’ cross plot from all wells (AA-2, AA-3 and AA-4). From this figure, it is known that good porosity sand can be separated by Poisson’s Ratio approximately 0.29. From these cross plots, we observe that:

- P-impedance of gas is < 19000 (ft/sec*gr/cc),
- P-impedance of oil is between 19000 and 22000 (ft/sec*gr/cc), and
- P-impedance of water is > 23000 (ft/sec*gr/cc).

4.2. Well Log to Seismic Correlation and Wavelet Extraction

A first-important step for seismic AVO modeling and inversion to acoustic impedance is the estimation of the seismic wavelet. The estimation of the seismic wavelet is, in simple terms, found by correlating the seismic trace with a synthetic trace that is computed from the well log acoustic impedance. When correlating the synthetic and seismic data, we must be ensured that any time shift between the two data takes into account. The time shifts were removed in two stages: first applying check-shot corrections to the well depth-time curve, and second manual stretching and squeezing of the well log synthetic to better match the seismic trace.

4.2.1. Checkshot Corrections

The depth-time table calculated from the sonic log is rarely sufficient to produce a model impedance that ties the seismic data properly for the following reasons: the seismic datum and log datum may be different, the average first layer velocity is not known, errors in the sonic log velocities produce cumulative errors in the calculated travel-times, the events on the seismic data may be miss-positioned due to migration

errors, the seismic data may be subject to time stretch caused by frequency-dependent absorption and short-period multiples.

A check shot table is a series of measurements of actual 2-way time for a set of depths. The difference in travel time between the integrated sonic and the check shot times is called the drift curve. The drift curve is modeled by either a straight-line fit (linear), a spline fit, or a polynomial fit. For AA-2, AA-3 and AA-4 wells, a spline fit was used. The check shot correction was applied in such a way that only the depth-time curve was changed. In this case, the sonic log values were not changed, thus maintaining the original reflection coefficients.

4.2.2. Wavelet Extraction.

Following check shot correction there is invariably a time variant residual time shift between the seismic data and the well log synthetic. This residual timing error must be removed before we can make an accurate estimate of the seismic wavelet phase. The residual timing errors are estimated using a synthetic with a wavelet that is zero-phase and has the amplitude spectrum of the seismic data. By visually correlating events on the seismic data with events on the synthetic, the synthetic is “stretched and squeezed” to better fit the seismic trace. This stretching and squeezing is applied as a residual check shot correction. After the residual check shot correction has been made, the full wavelet with both amplitude and phase spectra is estimated.

The wavelet extracted at AA-2, AA-3 and AA-4 wells are zero phase wavelet, shown in Figure-4.6 to Figure-4.8. These wavelets were used in the AVO modeling and the AVO inversion process. The well to seismic correlation at the AA wells location using a synthetic with the extracted wavelet from each wells are shown in Figure-4.9 to Figure-4.11.

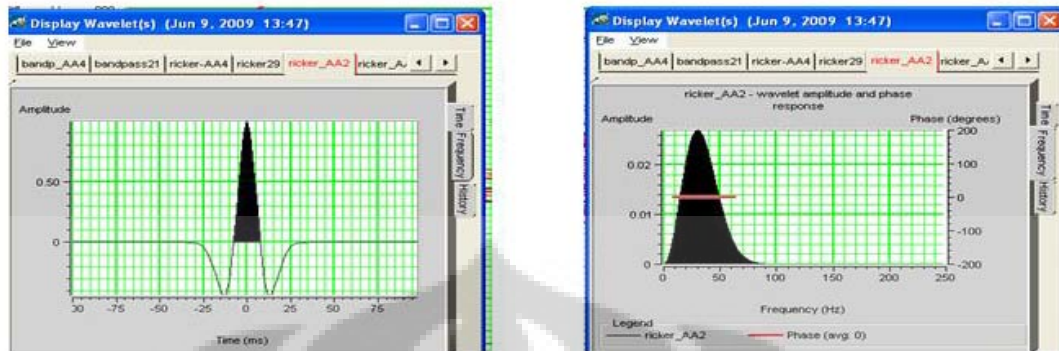


Figure-4.6: Wavelet of AA-2 well in Time and Frequency Domains.

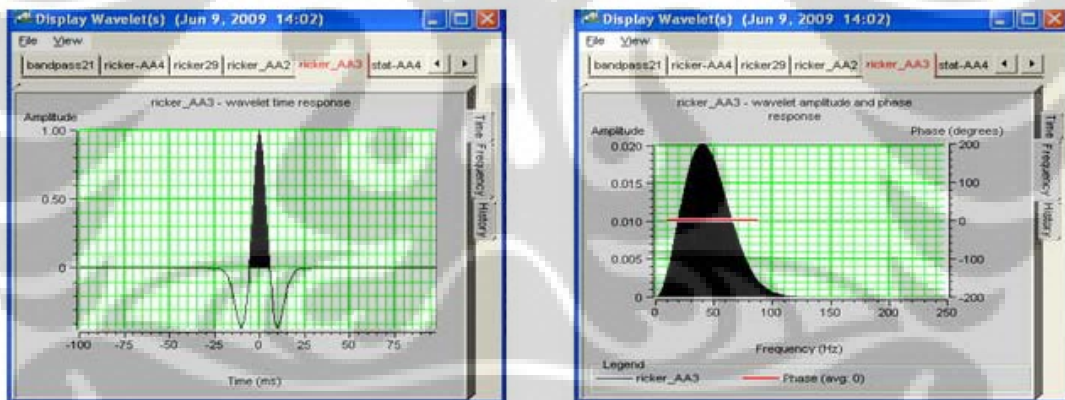


Figure-4.7: Wavelet of AA-3 well in Time and Frequency Domains.

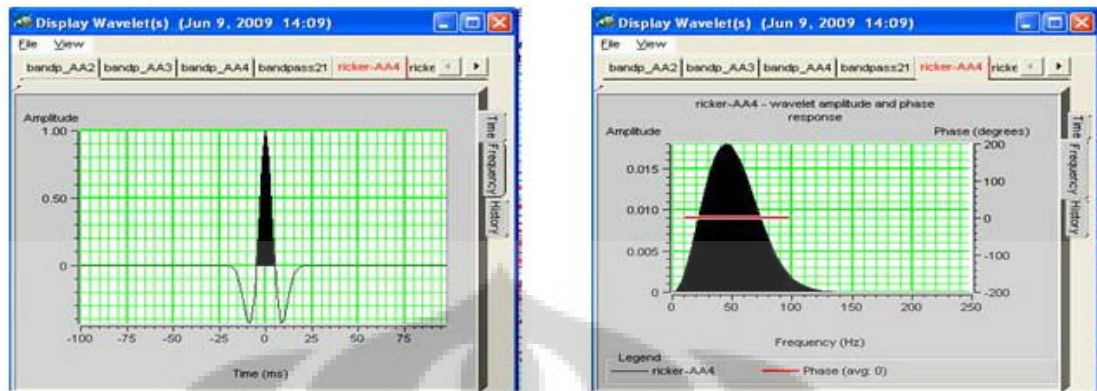


Figure-4.8: Wavelet of AA-4 well in Time and Frequency Domains.

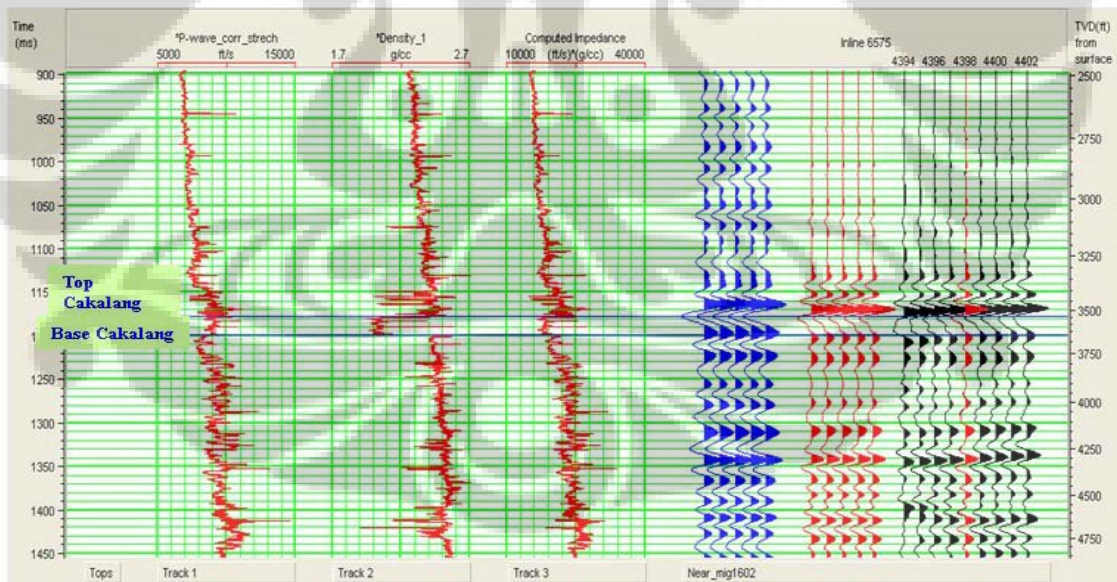


Figure-4.9: Good well to seismic correlation at the AA-2 well.

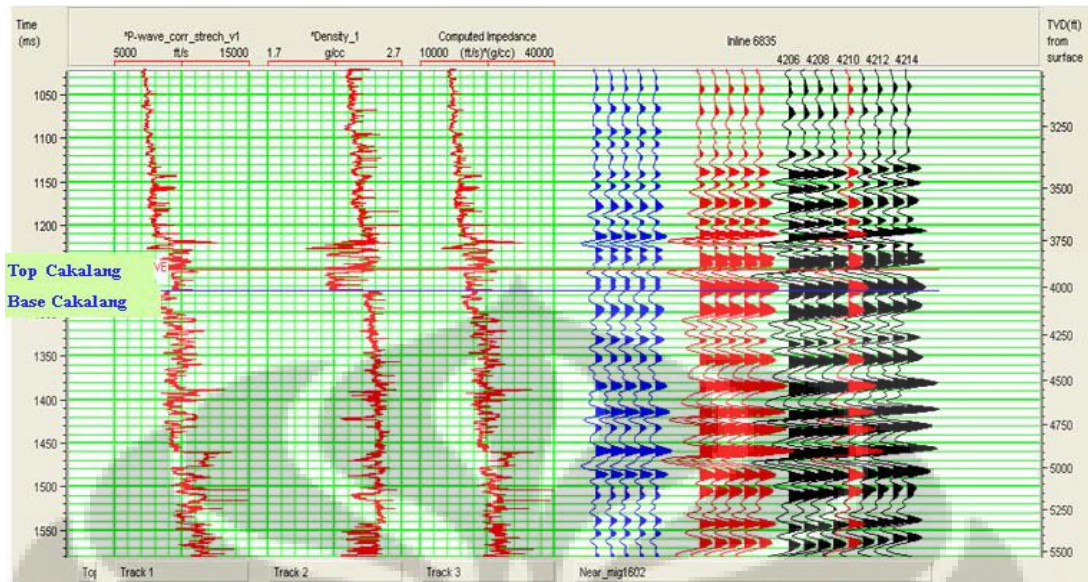


Figure-4.10: Good well to seismic correlation at the AA-3 well.

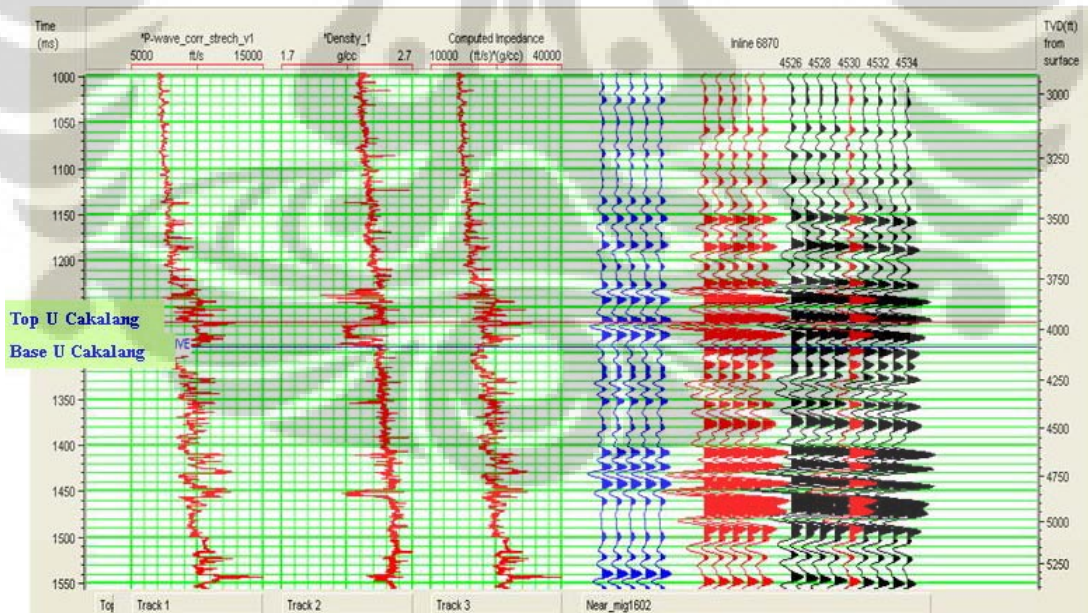


Figure-4.11: Good well to seismic correlation at the AA-3 well.

4.3. AVO Modeling.

Synthetic offset gathers were obtained for various fluid models in one zone for all wells. The zone boundary is listed in Table-1. The physical parameters of the models were based on the recorded P-wave velocity log, the recorded density log, the recorded S-wave log and the water saturation log.

Starting with the recorded logs and the fluid petrophysical properties, the Biot-Gassmann equations were used to perform fluid replacement. The recorded logs provide the data for the in-situ fluids model.

Well Name	Boundary	Depth from KB (feet)	Depth from Surface (feet)
AA-2	Top	3629	3547
	Base	3754	3672
AA-3	Top	3970	3905
	Base	4092	4027
AA-4	Top	4024	3959
	Base	4162	4097

Table-4.1: Zone Boundary for AVO modeling.

4.3.1. Fluid Replacement Modelling Procedure

The fluid replacement modeling using Biot Gasmann equation was performed for the wells AA-2, AA-3 and AA-4 using water saturation of 0%, 10%, 20%, 30%, 40%, 50%, 60%, 70%, 80%, 90% and 100. The results of changes in P-wave and S-wave from this procedure can be seen from Figure-4.12 to Figure-4.14. From these figures, we observe that P-waves changes more than S-wave, as S-velocity is not sensitive to fluids. Small changes in S-velocity is due to density effects.

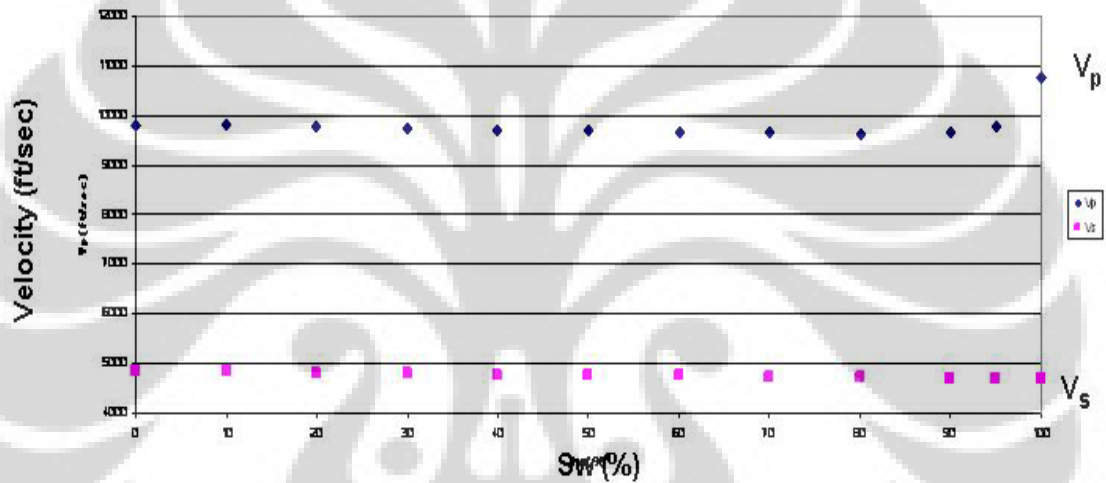


Figure-4.12: Vp and Vs in a gas sand at AA-2 well using Biot Gasmann.

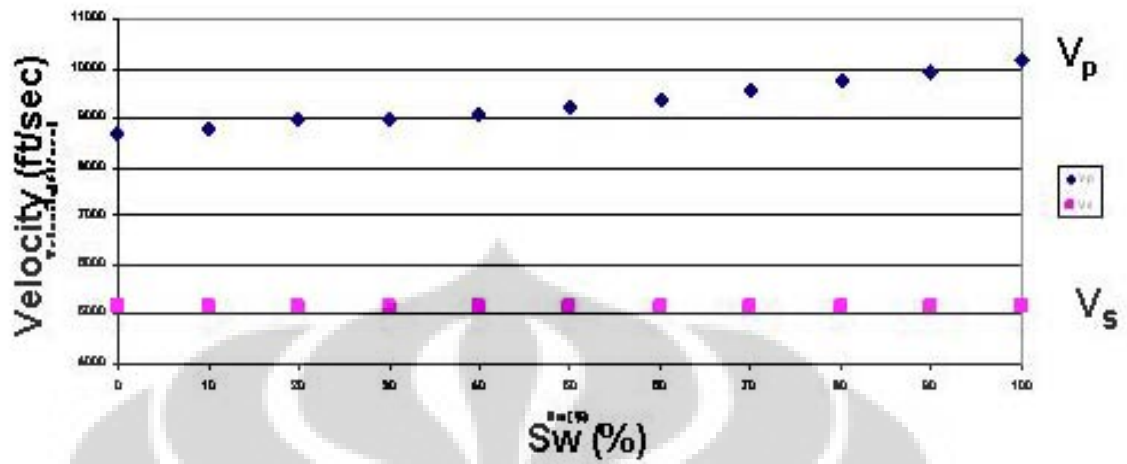


Figure-4.13: Vp and Vs in an oil sand at AA-3 well using Biot Gasmann.

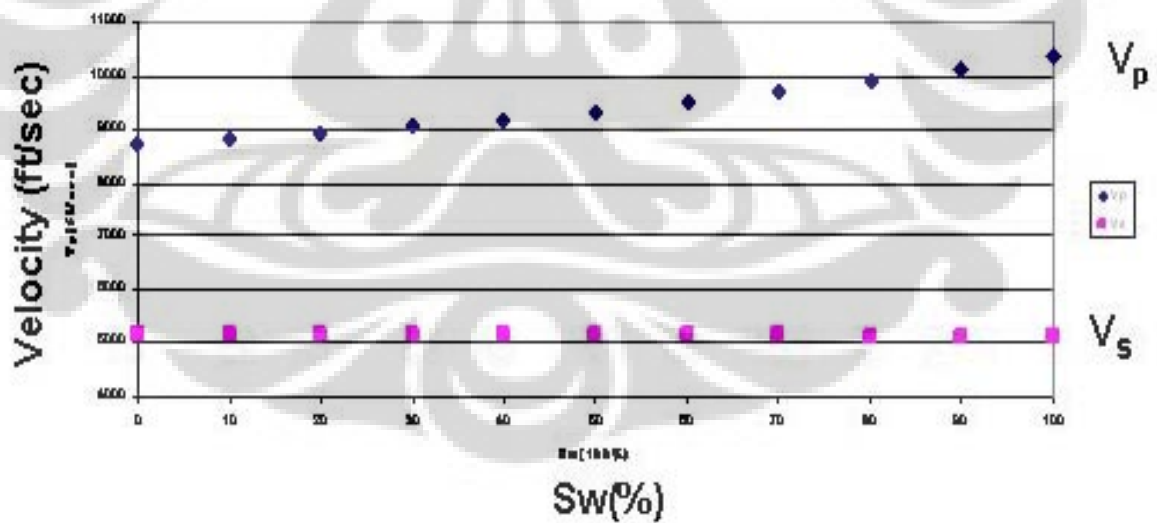


Figure-4.14: Vp and Vs in an oil-water sand at AA-4 well using Biot Gasmann.

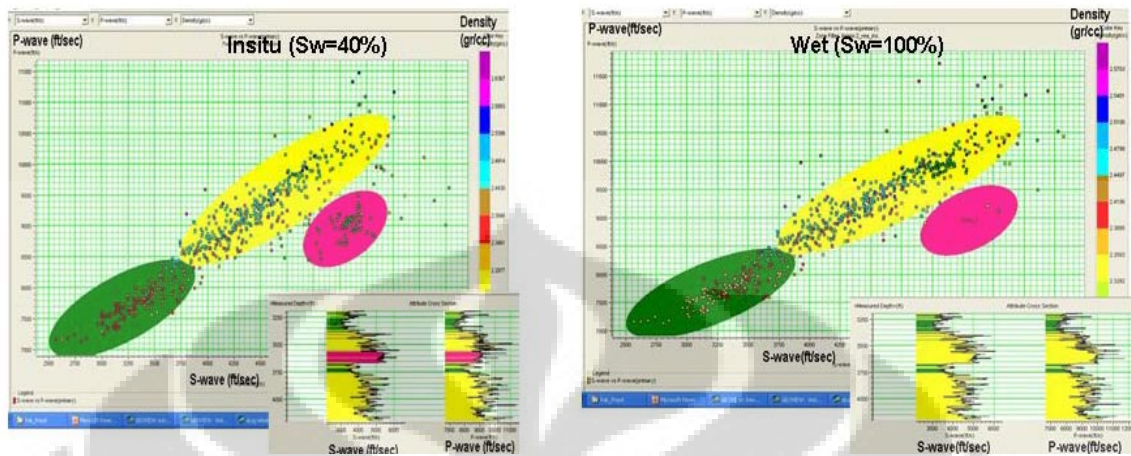


Figure-4.16: S-wave versus P-wave versus Density of AA-2 well (Insitu and Sw=100%).

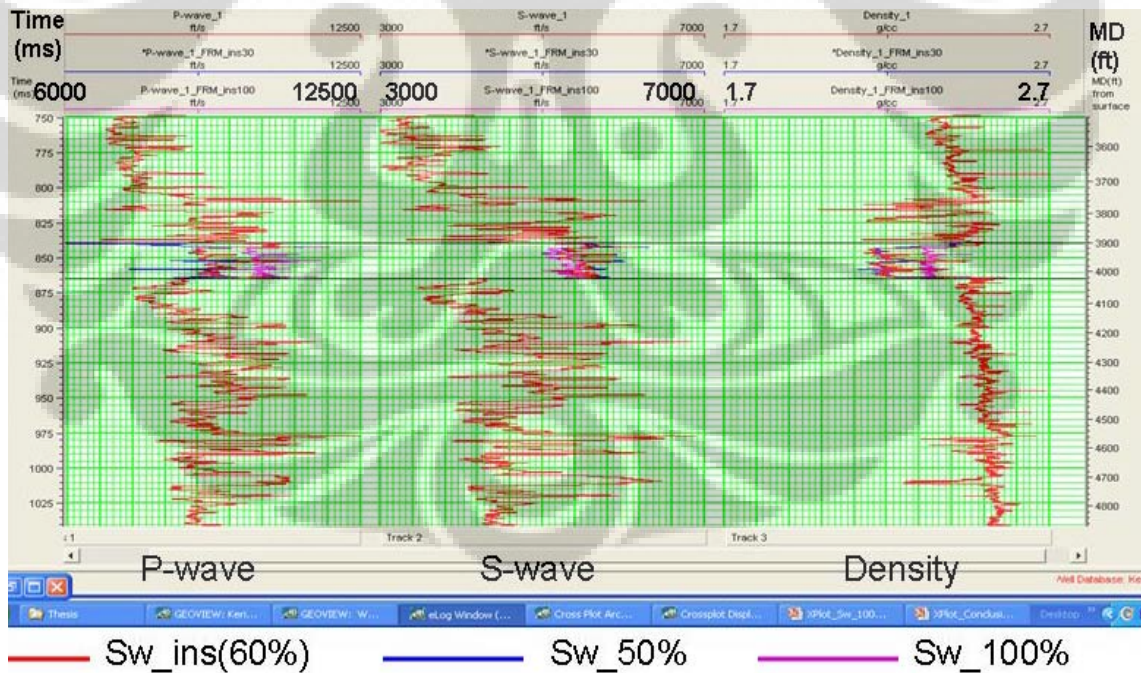


Figure-4.17: Fluid Replacement Modeling of AA-3 with water saturation 50% and 100%.

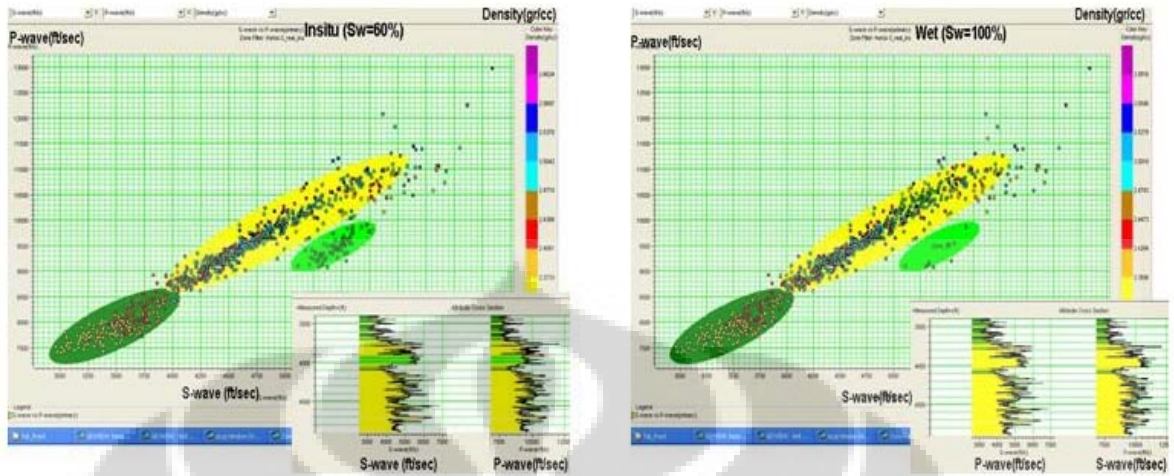


Figure-4.18: S-wave versus P-wave versus Density of AA-3 well (Insitu and Sw=100%).

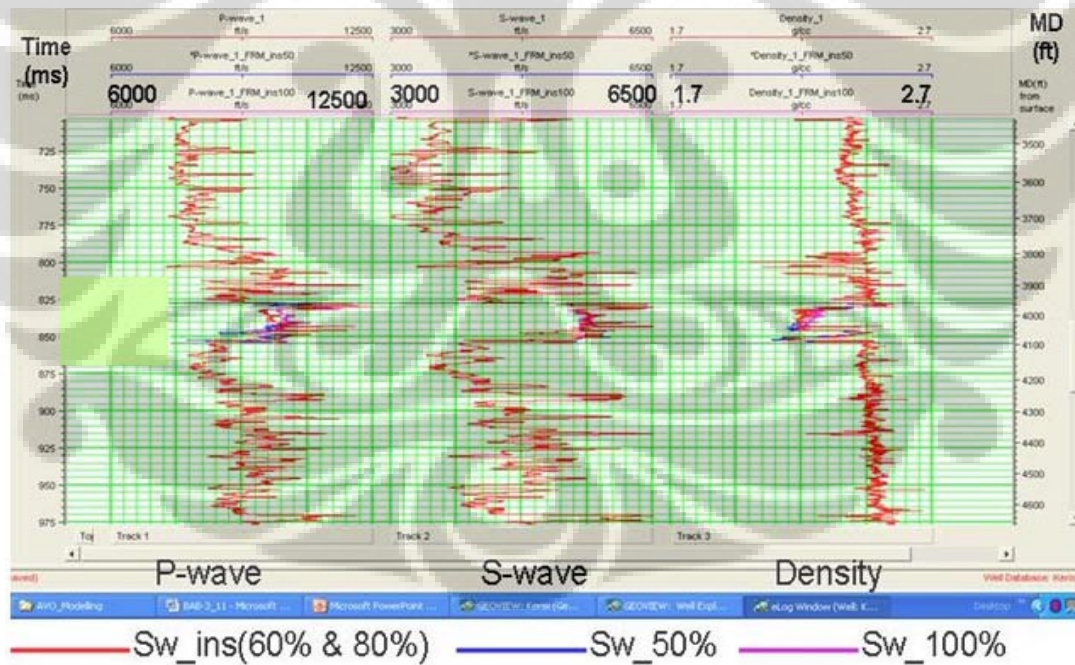


Figure-4.19: Fluid Replacement Modeling of AA-4 with water saturation 50% and 100%.

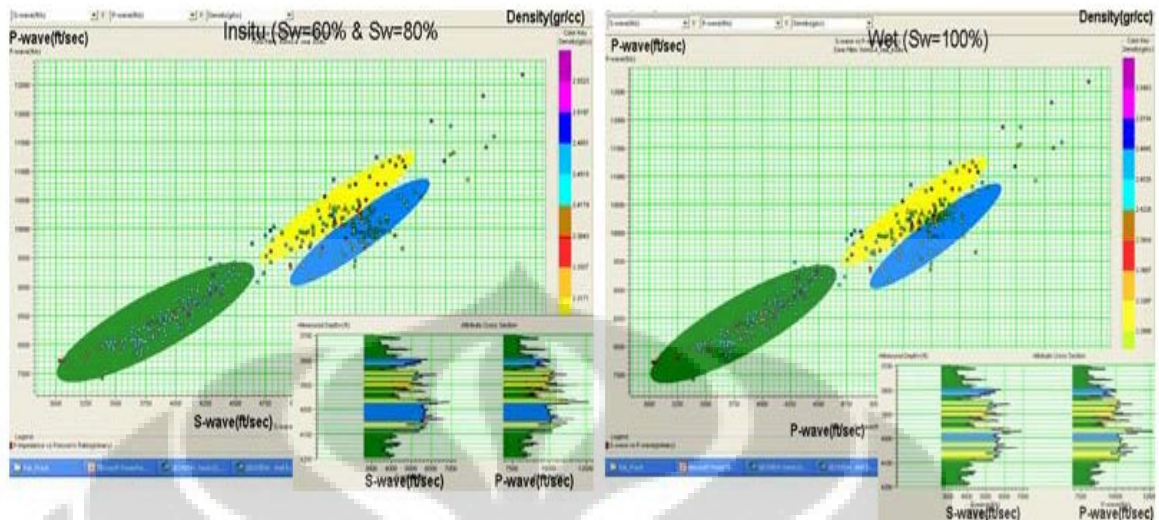


Figure-4.20: S-wave versus P-wave versus Density of AA-4 well (Insitu and Sw=100%).

4.3.2. 2D Synthetics

Synthetic offset gathers were generated for insitu case and wet case (Sw=100%) at each wells. The gathers were computed using the Zoeppritz equation. The Zoeppritz equation reflectivity and transmission coefficients of P-waves and S-waves to the angles of reflection and transmission and the densities across a single impedance boundary. The wavelets used were wavelets extracted from each wells.

Model of prestack synthetic seismogram computed from well log data and compared to the actual observed angle gather (near) show there is generally good match between the compute synthetic model and observe seismogram as shown in Figure-4.21 to Figure-4.23., which suggest that there is good correlation between the well log and seismic data, providing confidence in the soundness of the AVO method and its suitability for application in this portion of the AA field.

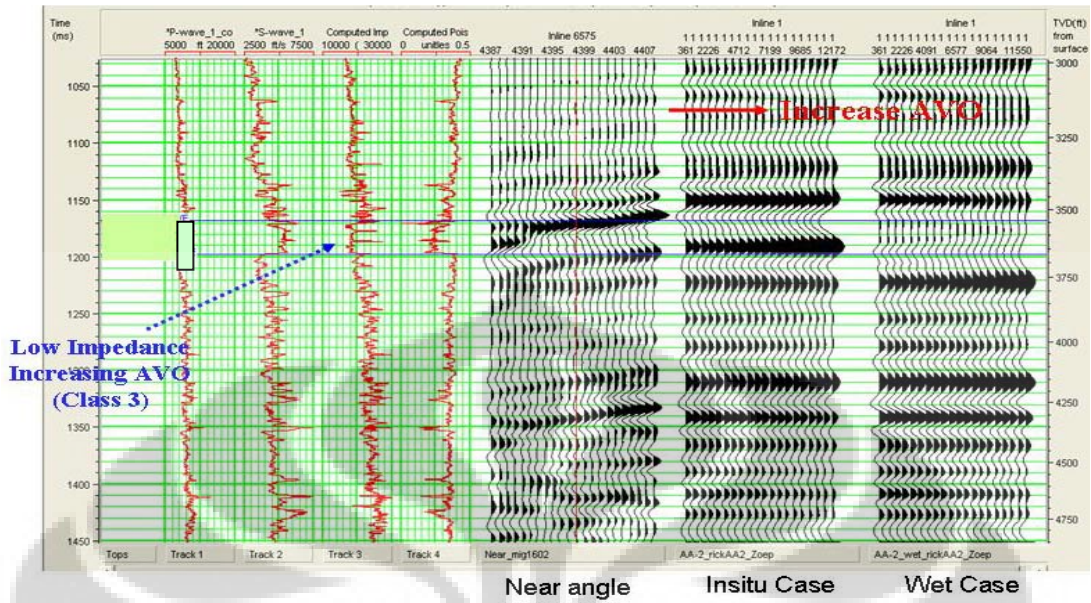


Figure-4.21: 2D Synthetics of AA-2 well (Insitu and Wet Cases).

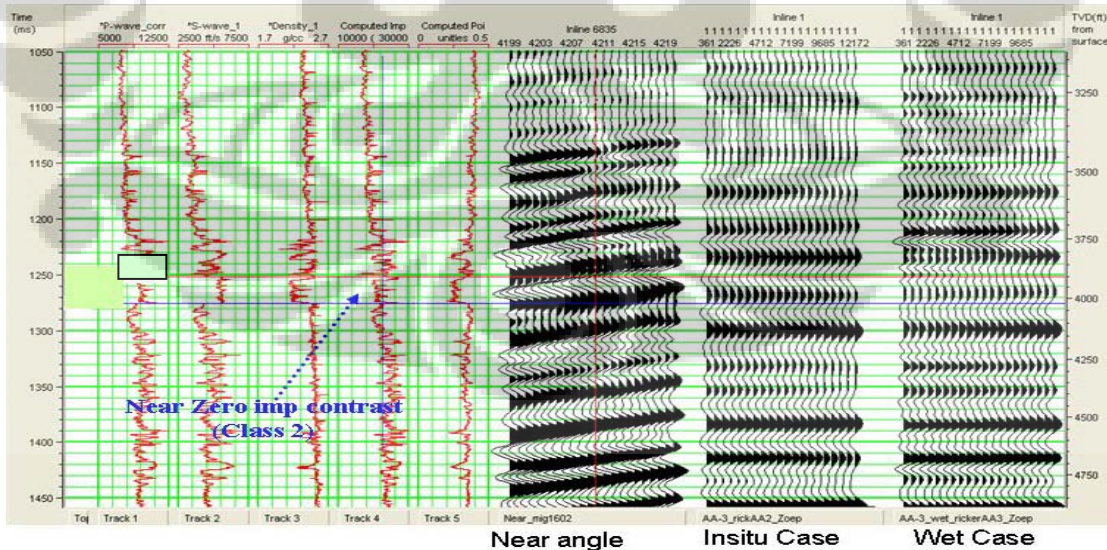


Figure-4.22: 2D Synthetics of AA-3 well (Insitu and Wet Cases).

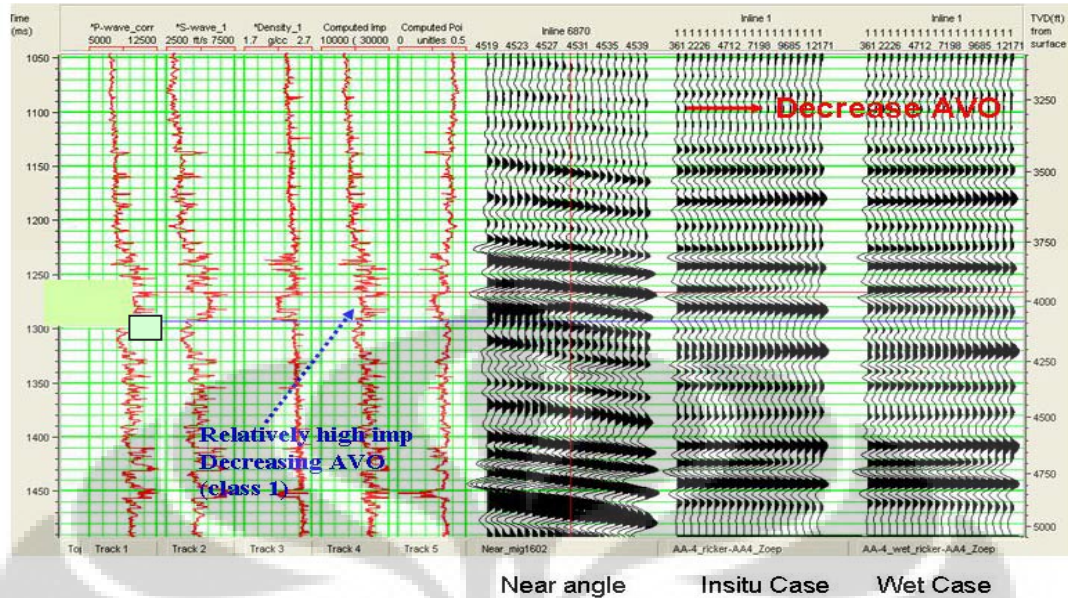


Figure-4.23: 2D Synthetics of AA-4 well (Insitu and Wet Cases).

As shown in Figure-4.21, amplitude versus offset (AVO) increases with offset and has low impedance in the zone of interest. Based on Rutherford and Williams classification, this is a Class III AVO anomaly. Figure-4.22 shows no change of AVO and the impedance contrast is close to zero, which is a Class II AVO anomaly. While Figure-4.23 shows AVO decreasing and relatively has high impedance, so this is a Class I AVO anomaly.

4.4. AVO Inversion

Through AVO inversion, data volumes of specific rock properties represented by seismic attributes were generated from amplitude with offset behavior derived from the partial stack seismic data. The AVO derived seismic data were calibrated to log measurements and then extrapolated away from the borehole throughout the volume.

Moreover, instead of an interface property, such as the reflection coefficient, meaningful numerical quantities associated with the reservoir may be obtained from the extracted data volume. Thus these derived AVO attributes are portable and both absolute and relative comparisons of AVO attributes are facilitated.

4.4.1. Initial Guess Model

The first step in the inversion is to create an initial model of P-impedance and S-impedances. These initial models were used to as the basis for inversion algorithms. In this thesis, Top Cakalang and Base Cakalang horizons were imported into the STRATA program.

The P and S impedance logs in time were interpolated following the horizons. The steps taken to ensure a good time tie between the well data and the seismic data was discussed in the previous section on check shot corrections and well to seismic correlation. The extracted wavelet is also an important component of the initial model.

The initial impedances model obtained through interpolation of the AA-2, AA3 and AA-4 impedances logs are shown in Figure-4.24 to Figure-4.26.

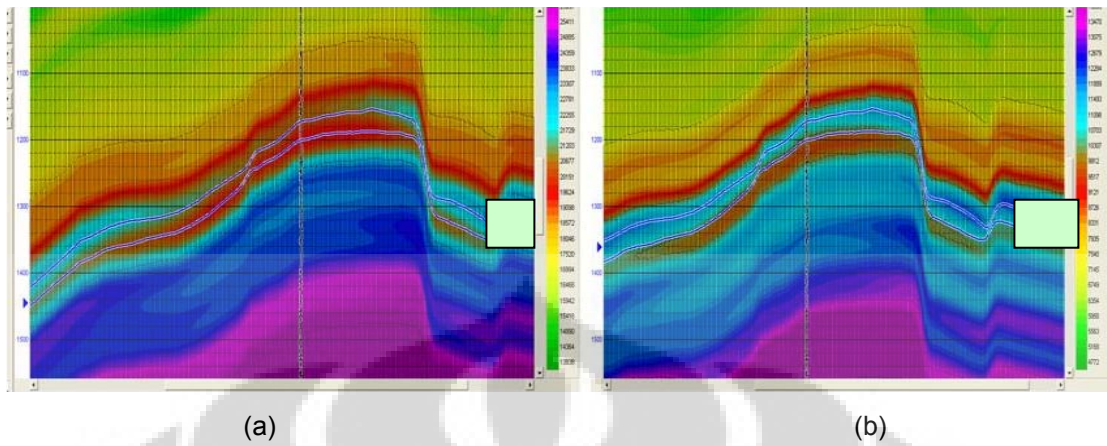


Figure-4.24: a. Initial P-impedance Model showing AA-2 well location.
 b. Initial S-impedance Model showing AA-2 well location.

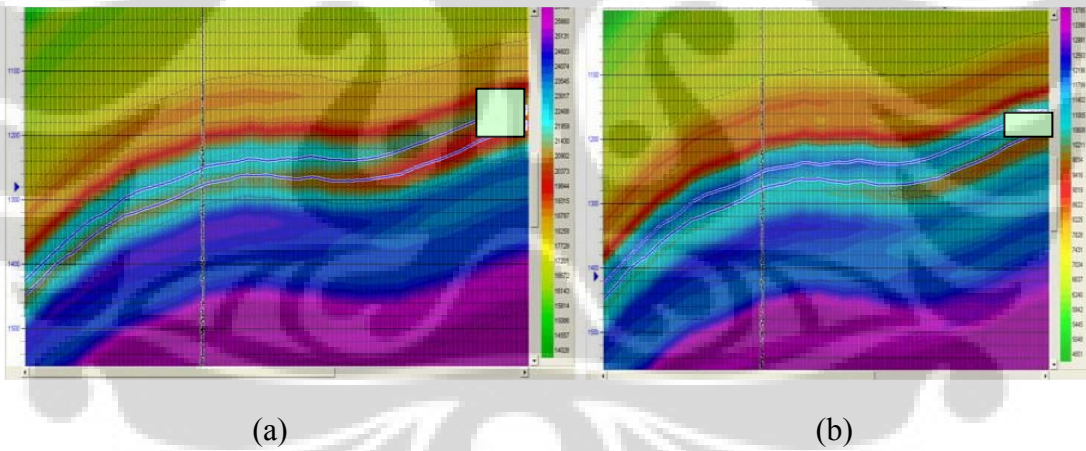


Figure-4.25: a. Initial P-impedance Model showing AA-3 well location.
 b. Initial S-impedance Model showing AA-3 well location.

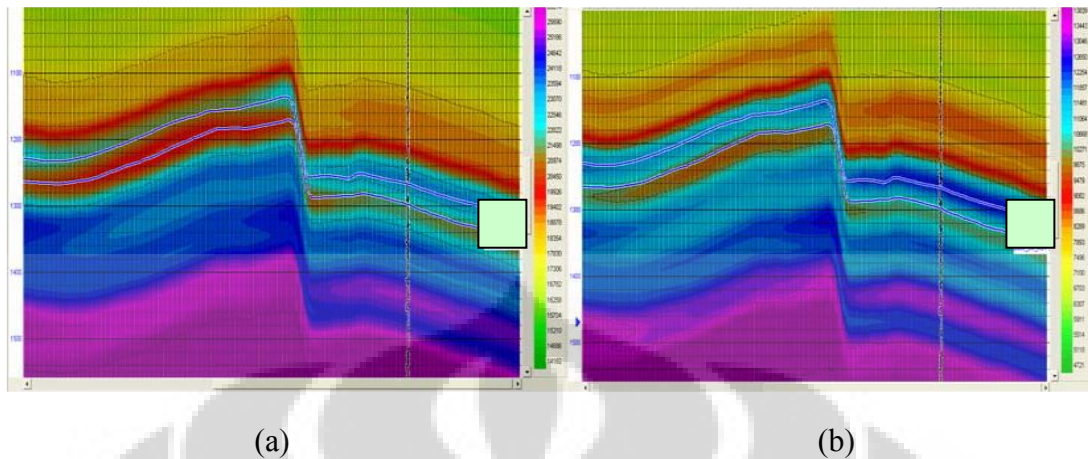


Figure-4.26: a. Initial P-impedance Model showing AA-4 well location.
 b. Initial S-impedance Model showing AA-4 well location.

4.4.2. Pre Stack Inversion

In this thesis, the workflow of the Pre Stack Inversion process is as follow:

Step 1: Created blocked initial impedance model within 1000 – 1500 ms time interval.

Step 2: Generated synthetic trace by convolving the blocky impedance with given wavelets.

Step 3: Compare the synthetic trace with the real trace as shown in Figure-4.27 to Figure-4.29.

Step 4: Modify the impedance model through iteration to meet objective function, which is improve the fit that has small errors between calculated synthetic of the model and real seismic data.

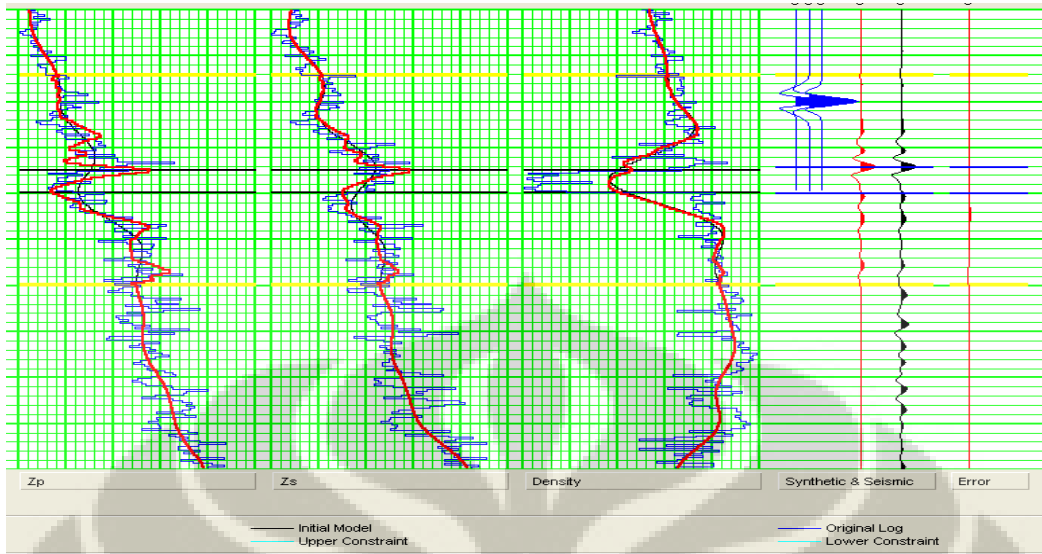


Figure-4.27: The fit between the inversion traces and the original logs for AA-2.

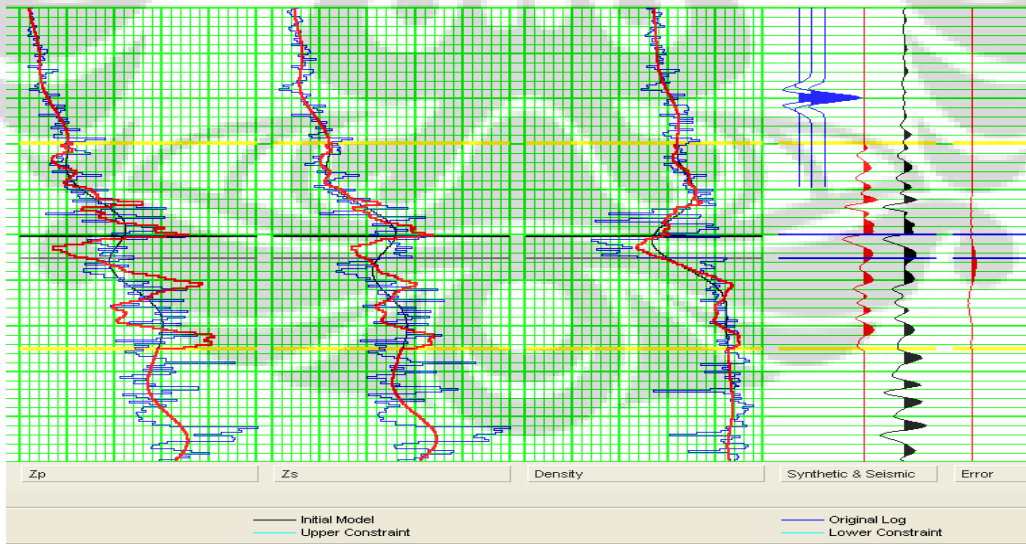


Figure-4.28: The fit between the inversion traces and the original logs for AA-3.

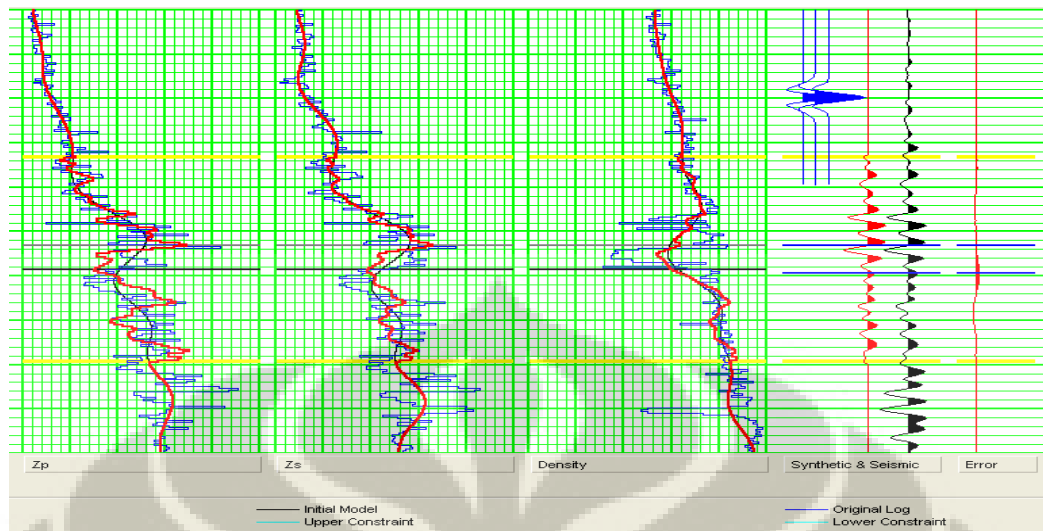


FIGURE-4.29: The fit between the inversion traces and the original logs for AA-4.

The results of the inversion are P-impedance (Z_p), V_p/V_s volumes, and Poisson Ratio (PR) volumes. A cross plot between Z_p and PR were then generated. To see the distribution of fluids and lithology, rock physics template (filter) shown in Figure-4.5 was used and the pictures can be seen in Figure-4.30 to Figure-4.33. While horizon slice on Top Cakalang of Z_p and PR volumes can be seen in Figure-4.34 and Figure-4.35.

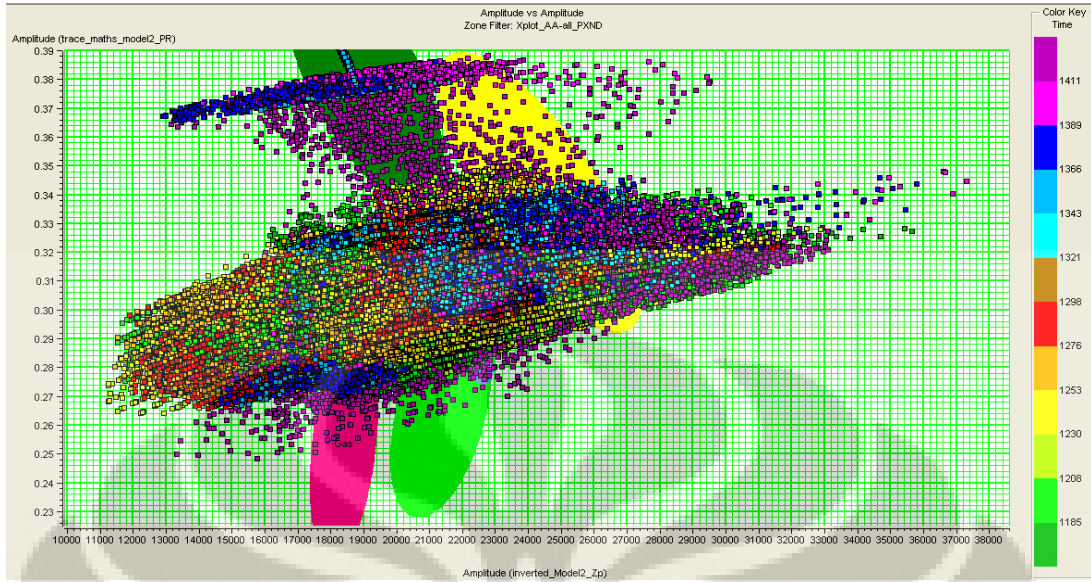


Figure-4.30: Amplitude Zp versus Amplitude PR.

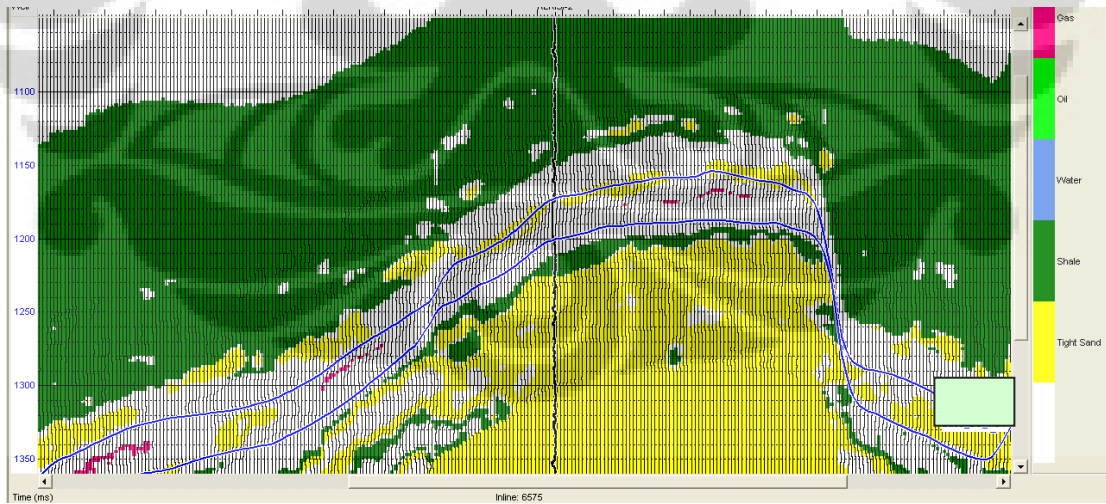


Figure-4.31: Fluids and lithology distribution at AA-2 well.

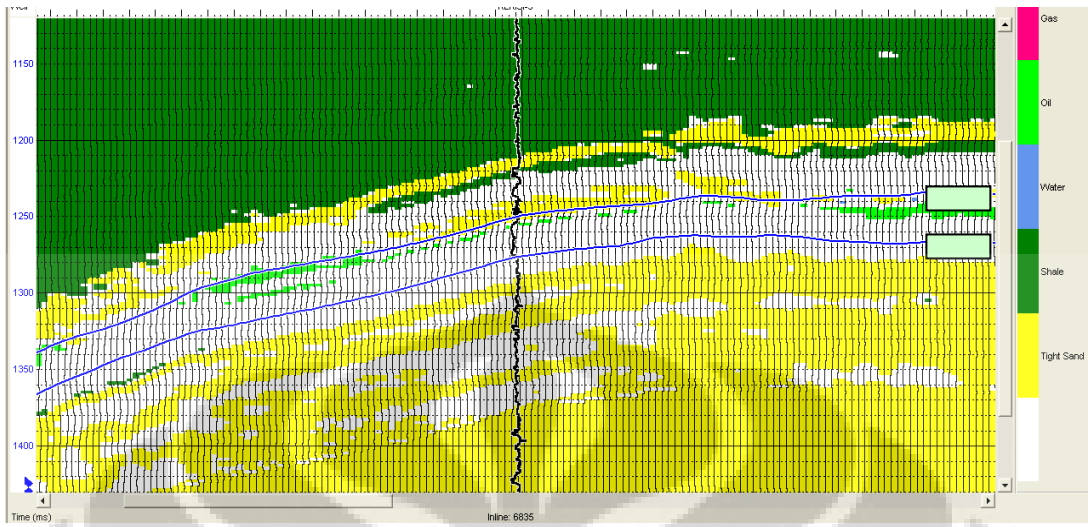


Figure-4.32: Fluids and lithology distribution at AA-3 well.

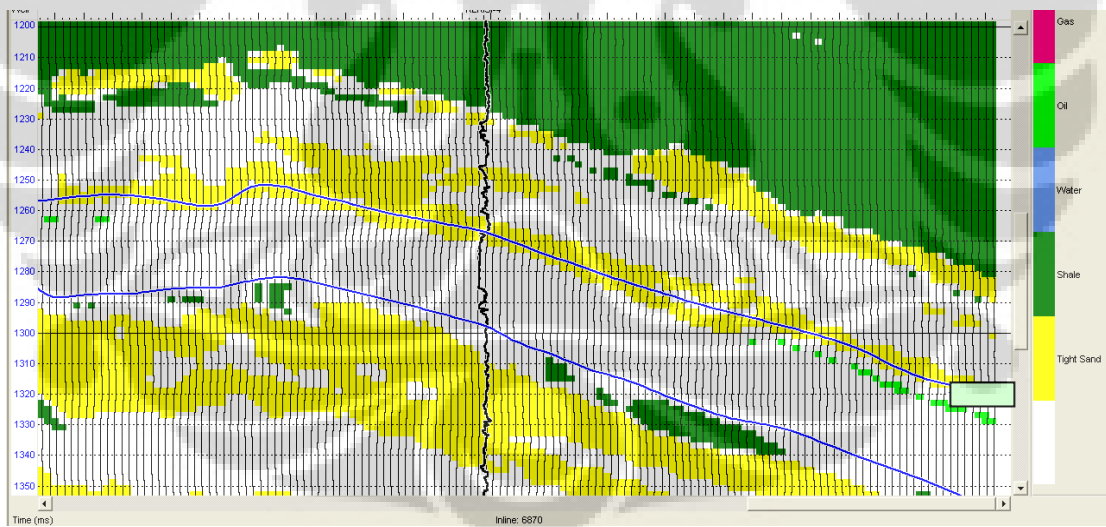


Figure-4.33: Fluids and lithology distribution at AA-4 well.

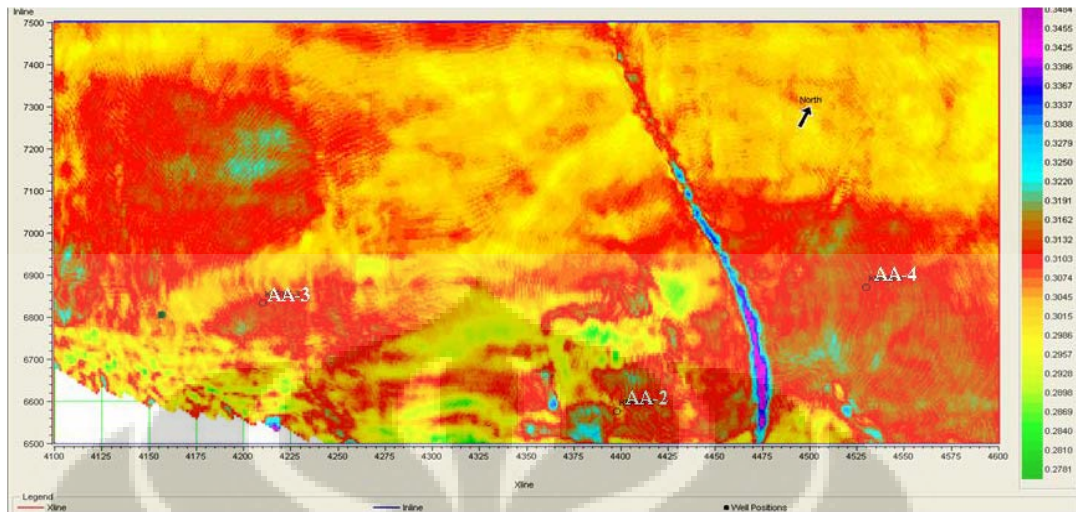


Figure-4.34: Horizon slice on Top Cakalang of Zp volume.

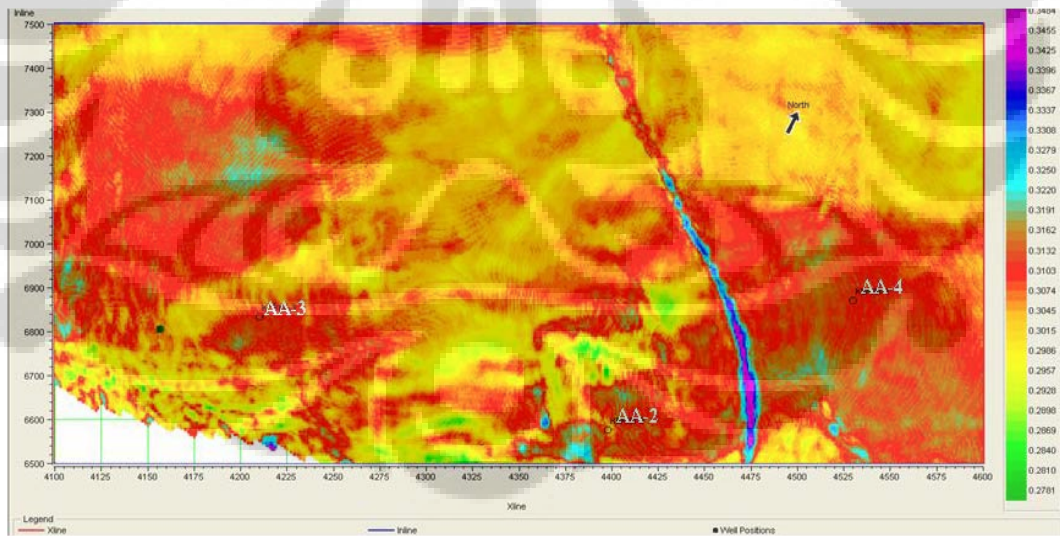


Figure-4.35: Horizon slice on Top Cakalang of PR volume.

CHAPTER V

CONCLUSION AND RECOMENDATION

5.1. Conclusion

Conclusions of the thesis are:

1. From log analysis, we observe that a cross plot between P-impedance versus Poisson Ratio can separate different lithology and fluid, i.e: good porosity sand has low P-impedance and low Poisson Ratio; gas sand has lower P-impedance and Poisson Ratio compare to oil and gas, etc.
2. AVO synthetics were generated and classified at each well location, i.e: Well AA-2 is interpreted as Class III AVO, whereas Well AA-3 is interpreted as Class II AVO.
3. P-impedance and Poisson Ratio seismic volumes have been generated through seismic inversion process incorporating many inputs, such as pre-stack seismic volumes; P and S velocity and density logs from well; interpreted horizons; and extracted wavelets.
4. Based on the AVO inversion results (P-impedance and Poisson Ratio volumes) tied to AVO classification and cross plots from log analysis, further interpretation for lithology and fluid distribution can be carried-out for a better results compare to normal seismic reflectivity volumes.

5.2. Recommendation

Recommendations of the thesis are:

1. Further inversion may need to investigate the use of a single wavelet that captures seismic frequencies (30-40 hz) within the interval of interest.
2. A scalar may need to be applied so that we have comparable values between seismic inversion results and log data for better quality control.

REFERENCE

Avseth, Per., Mukerji Tapan., Mavko, Gary., Quantitative Seismic Interpretation, Applying Rock Physics Tools to Reduce Interpretation Risk, Cambridge University Press.

Fatti, Jan L., Smith, George C., Vail, Peter J., Strauss, Peter J., and Levitt, Phillip R., Detection of Gas in Sandstone Reservoirs using AVO Analysis: A 3-D Seismic Case History using the Geostack Technique.

Hilterman, F.J., 2001, Seismic Amplitude Interpretation, 2001 Distinguished Instructor Short Course, Series, No.4, Sponsored by SEG & EAGE.

Munadi, Suprayitno, Dr., Aspek Fisis Seismologi Eksplorasi, Program Studi Geofisika, Jurusan Fisika FMIPA, Universitas Indonesia, Depok, 2000.

Nefrizal., Munadi, Suprayitno., Numerical Modeling of Seismic Wave Propagation in Porous Media, LEMIGAS SCIENTIFIC CONTRIBUTION, 2/97.

Russel, Hampson, AVO Workshop Part 1 & 2, A CGG Veritas Company, CGG Veritas.

Russell, Brian H., Hedlin, Ken., Hilterman, Fred J., and Lines, Lawrence R., Fluid Property Discrimination with AVO: A Biot-Gassmann Perspective, Geophysics Vol 68, No 1 (January-February).

Russell, Brian, M.Sc., P.Geoph, Practical AVO, Humpson Russell Software Service Ltd, Calgary, Canada.

Young, Kathryn., Tatham, Robert H., Jackson School of Geosciences, University of Texas-Austin, Austin, USA, Fluid Discrimination of Poststack “Bright Spot” in The Columbus Basin, Offshore Trinidad, The Leading Edge, December, 2007.

